Commun. Comput. Phys.
doi: 10.4208/cicp.OA-2021-0074

Vol. **31**, No. 1, pp. 60-93
January 2022

A Modified Crank-Nicolson Numerical Scheme for the Flory-Huggins Cahn-Hilliard Model

Wenbin Chen[1,2], Jianyu Jing[2], Cheng Wang[3], Xiaoming Wang[4,*] and Steven M. Wise[5]

[1] *Shanghai Key Laboratory for Contemporary Applied Mathematics, Fudan University, Shanghai 200433, P.R. China.*
[2] *School of Mathematical Sciences, Fudan University, Shanghai 200433, P.R. China.*
[3] *Mathematics Department, University of Massachusetts, North Dartmouth, MA 02747, USA.*
[4] *International Center for Mathematics and Department of Mathematics, and Guangdong Provincial Key Laboratory of Computational Science and Material Design, and National Center for Applied Mathematics Shenzhen, Southern University of Science and Technology, Shenzhen 518055, P.R. China.*
[5] *Mathematics Department, University of Tennessee, Knoxville, TN 37996, USA.*

Received 11 April 2021; Accepted (in revised version) 7 September 2021

Abstract. In this paper we propose and analyze a second order accurate numerical scheme for the Cahn-Hilliard equation with logarithmic Flory Huggins energy potential. A modified Crank-Nicolson approximation is applied to the logarithmic nonlinear term, while the expansive term is updated by an explicit second order Adams-Bashforth extrapolation, and an alternate temporal stencil is used for the surface diffusion term. A nonlinear artificial regularization term is added in the numerical scheme, which ensures the positivity-preserving property, i.e., the numerical value of the phase variable is always between -1 and 1 at a point-wise level. Furthermore, an unconditional energy stability of the numerical scheme is derived, leveraging the special form of the logarithmic approximation term. In addition, an optimal rate convergence estimate is provided for the proposed numerical scheme, with the help of linearized stability analysis. A few numerical results, including both the constant-mobility and solution-dependent mobility flows, are presented to validate the robustness of the proposed numerical scheme.

AMS subject classifications: 35K35, 35K55, 49J40, 65K10, 65M06, 65M12

Key words: Cahn-Hilliard equation, Flory Huggins energy potential, positivity preserving, energy stability, second order accuracy, optimal rate convergence estimate.

*Corresponding author. *Email addresses:* wbchen@fudan.edu.cn (W. Chen), 20110180021@fudan.edu.cn (J. Jing), cwang1@umassd.edu (C. Wang), wxm.math@outlook.com (X. Wang), swise1@utk.edu (S. M. Wise)

1 Introduction

The Allen-Cahn (AC) [3] and Cahn-Hilliard (CH) [9] equations are fundamental gradient flow models in the description of phase transitions. For any $\phi\in H^1(\Omega)$, the Cahn-Hilliard-Flory-Huggins energy functional is formulated as

$$E(\phi)=\int_\Omega\left((1+\phi)\ln(1+\phi)+(1-\phi)\ln(1-\phi)-\frac{\theta_0}{2}\phi^2+\frac{\varepsilon^2}{2}|\nabla\phi|^2\right)d\mathbf{x}, \tag{1.1}$$

where $\Omega\subset\mathbb{R}^d$ ($d=2$ or $d=3$) is a bounded domain and the point-wise bound $-1\le\phi\le1$ is assumed for phase field variable ϕ. The physical parameters $\varepsilon>0$ and $\theta_0>0$ are associated with the diffuse interface width and the temperature, respectively. The CH equation is an H^{-1}-like conserved gradient flow of the energy functional (1.1):

$$\partial_t\phi=\nabla\cdot(\mathcal{M}(\phi)\nabla\mu), \tag{1.2}$$

$$\mu:=\delta_\phi E=\ln(1+\phi)-\ln(1-\phi)-\theta_0\phi-\varepsilon^2\Delta\phi, \tag{1.3}$$

where $\mathcal{M}(\phi)>0$ stands for the mobility function. As a consequence, the gradient structure indicates an energy dissipation law: $\frac{d}{dt}E(\phi(t))=-\int_\Omega\mathcal{M}(\phi)|\nabla\mu|^2d\mathbf{x}\le0$. See the related references [8, 19, 23, 28]. In this article, we assume that $\Omega=(0,1)^3$, and consider periodic boundary conditions, for simplicity of presentation. An extension of our results for the model with homogeneous Neumann boundary conditions is straightforward.

Of course, the most visible difficulty for the Cahn-Hilliard equation (1.2) with logarithmic Flory Huggins energy potential is associated with the singularity in its derivative as the value of ϕ approaches -1 or 1. In fact, the positivity property, i.e., $0<1-\phi$ and $0<1+\phi$, has been established at the PDE analysis level in [2, 20, 28, 53]. As a further development, a separation property has also been justified for the 1-D and 2-D equations at a theoretical level. This property guarantees that a uniform distance exists between the value of the phase variable and the singular limit values. Such a distance only depends on ε, θ_0 and the initial data. See also the related works [1, 4, 18, 28, 33, 34, 52], et cetera. The free energy with the logarithmic pattern is considered in many cases to be more physically realistic than the regularly use polynomial version [23].

Regarding numerical approximation of the Cahn-Hilliard equation (1.2) with the Flory-Huggins energy (1.1), there have been extensive works [29, 41–43, 47, 54–56, 58, 61, 65], et cetera. Among the existing works, it is worth mentioning the pioneering work [19], which addresses the issue of the positivity-preserving property (for $1+\phi$ and $1-\phi$) when the implicit Euler scheme is applied and analyzed. Meanwhile, a time step constraint, $\Delta t\le\frac{4\varepsilon^2}{\theta_0^2}$, must be assumed, which comes from the implicit treatment of the expansive term. An extension to the multi-component Cahn-Hilliard flow has also been reported in [7].

A more recent work [13] has overcome the time step restriction, making use of the convex-concave decomposition approach. The positivity-preserving property, unique

solvability, and unconditional energy stability have been theoretically established for this convex splitting scheme. In particular, an implicit treatment of the nonlinear and singular logarithmic term played an essential role in the theoretical analysis, since the convex and the singular nature of the implicit logarithmic part prevents the numerical solution from approaching the singular values of -1 and 1. Similar ideas have been applied to other gradient models singular energy potential, such as the Cahn-Hilliard model with Flory-Huggins-deGennes energy potential [25–27, 66], the Poisson-Nernst-Planck system [50, 57], the reaction-diffusion system with detailed balance [49], a liquid film droplet model [68], et cetera.

Meanwhile, the work regarding second order accurate in time, energy stable schemes is very limited for the gradient flows with singular energy potentials. In this article, we propose and analyze a second order accurate scheme for the Cahn-Hilliard equation (1.2) with logarithmic Flory Huggins energy potential (1.1), based on a modified Crank-Nicolson temporal discretization, combined with the finite difference spatial approximation. In more details, a modified Crank-Nicolson (secant-like) approximation is applied to the logarithmic nonlinear term, which takes the form

$$\frac{F(1\pm\phi^{n+1})-F(1\pm\phi^{n})}{\phi^{n+1}-\phi^{n}},\quad \text{with}\quad F(x)=x\ln x.$$

Such an approximation is convex in terms of ϕ^{n+1}, though the approximation is not singular as $\phi^{n+1}\searrow -1$ or $\phi^{n+1}\nearrow 1$. The expansive term is updated by a second order Adams-Bashforth explicit extrapolation formula, and an alternate temporal stencil, namely,

$$\frac{3}{4}\Delta_h\phi^{n+1}+\frac{1}{4}\Delta_h\phi^{n-1},$$

is used for the surface diffusion (diffuse interface) term. Since the singularity of the nonlinear approximation to the logarithmic term is not available as $\phi^{n+1}\searrow -1$ or $\phi^{n+1}\nearrow 1$, we add a nonlinear artificial regularization term, in the form of

$$\Delta t(\ln(1\pm\phi^{n+1})-\ln(1\pm\phi^{n})),$$

in the numerical scheme. Such a regularization term, we will show, ensures the positivity-preserving property for both $1+\phi$ and $1-\phi$ at a point-wise level. In particular, the singular nature of the logarithmic terms around the values of -1 and $+1$ prevents the numerical solution reaching these singular values. An unconditional energy stability of the numerical scheme is derived, based on the special form of the logarithmic approximation term.

An optimal rate convergence analysis for the proposed numerical scheme turns out to be very challenging. This is due to the fact that a highly nonlinear approximation to the logarithmic chemical potential is involved with both ϕ^{n+1} and ϕ^{n} in the modified Crank-Nicolson temporal discretization. To overcome this difficulty, we perform a discrete $L^{\infty}_{\Delta t}(0,T;H_h^{-1})\cap L^{2}_{\Delta t}(0,T;H_h^{1})$ error estimate. The $\frac{3}{4}$ and $\frac{1}{4}$ coefficient distribution

for the surface diffusion term makes an additional dissipation available that is able to control the numerical errors associated with the nonlinear logarithmic and the concave expansive terms. In addition, the numerical error associated with the highly nonlinear logarithmic terms is decomposed into two parts, corresponding to the time steps t_n and t_{n+1}, respectively. The numerical error part corresponding to the time step t_{n+1} is proven to be non-positive, due to the convex nature of the implicit term. Meanwhile, the numerical error part corresponding to t_n could be bounded with the help of linearized stability analysis, combined with the separation property. All these techniques lead to the optimal rate error estimate, with $\mathcal{O}(\Delta t^2+h^2)$ accuracy order.

The rest of the article is organized as follows. In Section 2 we propose the numerical scheme and state the corresponding theoretical results. The detailed proof for the positivity-preserving property is provided in Section 3, and the modified energy stability is proved in Section 4. The optimal rate convergence analysis is presented in Section 5. Subsequently, the preconditioned steepest descent (PSD) iteration solver is outlined in Section 6. Some numerical results are presented in Section 7. Finally, concluding remarks are given in Section 8.

2 The numerical scheme and the main theoretical results

2.1 The finite difference spatial discretization

The standard centered finite difference spatial approximation is applied. We present the numerical approximation on the computational domain $\Omega=(0,1)^3$ with a periodic boundary condition, and $\Delta x=\Delta y=\Delta z=h=\frac{1}{N}$ with $N\in\mathbb{N}$ to be the spatial mesh resolution throughout this work. In particular, $f_{i,j,k}$ stands for the numerical value of f at the cell centered mesh points $((i+\frac{1}{2})h,(j+\frac{1}{2})h,(k+\frac{1}{2})h)$, and we denote $\mathcal{C}_{\rm per}$ as

$$\mathcal{C}_{\rm per}:=\left\{f:\mathbb{Z}^3\to\mathbb{R}\;\middle|\; f_{i,j,k}=f_{i+\alpha N,j+\beta N,k+\gamma N},\ \forall i,j,k,\alpha,\beta,\gamma\in\mathbb{Z}\right\},$$

with the discrete periodic boundary condition imposed. In turn, the discrete average and difference operators are face-centered functions, evaluated at the east-west faces, $(i+1/2,j,k)$; north-south faces, $(i,j+1/2,k)$; and up-down faces, $(i,j,k+1/2)$, respectively:

$$\begin{aligned}
&A_x f_{i+1/2,j,k}:=\frac{1}{2}\left(f_{i+1,j,k}+f_{i,j,k}\right),\quad D_x f_{i+1/2,j,k}:=\frac{1}{h}\left(f_{i+1,j,k}-f_{i,j,k}\right),\\
&A_y f_{i,j+1/2,k}:=\frac{1}{2}\left(f_{i,j+1,k}+f_{i,j,k}\right),\quad D_y f_{i,j+1/2,k}:=\frac{1}{h}\left(f_{i,j+1,k}-f_{i,j,k}\right),\\
&A_z f_{i,j,k+1/2}:=\frac{1}{2}\left(f_{i,j,k+1}+f_{i,j,k}\right),\quad D_z f_{i,j,k+1/2}:=\frac{1}{h}\left(f_{i,j,k+1}-f_{i,j,k}\right).
\end{aligned}$$

Conversely, the corresponding operators at the staggered mesh points are defined as follows:

$$a_x f^x_{i,j,k} := \frac{1}{2}\left(f^x_{i+1/2,j,k} + f^x_{i-1/2,j,k}\right), \quad d_x f^x_{i,j,k} := \frac{1}{h}\left(f^x_{i+1/2,j,k} - f^x_{i-1/2,j,k}\right),$$
$$a_y f^y_{i,j,k} := \frac{1}{2}\left(f^y_{i,j+1/2,k} + f^y_{i,j-1/2,k}\right), \quad d_y f^y_{i,j,k} := \frac{1}{h}\left(f^y_{i,j+1/2,k} - f^y_{i,j-1/2,k}\right),$$
$$a_z f^z_{i,j,k} := \frac{1}{2}\left(f^z_{i,j,k+1/2} + f^z_{i,j,k-1/2}\right), \quad d_z f^z_{i,j,k} := \frac{1}{h}\left(f^z_{i,j,k+1/2} - f^z_{i,j,k-1/2}\right).$$

Suppose that g is any scalar function defined at all three faces (east-west, north-south, and up-down) and $\vec{f} = (f^x, f^y, f^z)^T$ a vector function, with f^x, f^y and f^z evaluated at the east-west face, $(i+1/2, j, k)$; north-south faces, $(i, j+1/2, k)$; and up-down faces, $(i, j, k+1/2)$, respectively. Then the discrete divergence is defined as

$$\nabla_h \cdot \left(g\vec{f}\right)_{i,j,k} = d_x \left(g_{\text{ew}} f^x\right)_{i,j,k} + d_y \left(g_{\text{ns}} f^y\right)_{i,j,k} + d_z \left(g_{\text{ud}} f^z\right)_{i,j,k}. \tag{2.1}$$

We use the notation $\vec{\mathcal{E}}_{\text{per}}$ to denote the set of all face-centered vector grid functions $\vec{f} = (f^x, f^y, f^z)^T$ that are Ω-periodic, that is, N-periodic in each dimension.

In particular, if $\vec{f} = \nabla_h \phi = (D_x\phi, D_y\phi, D_z\phi)^T$ for certain scalar grid function ϕ, the corresponding divergence becomes

$$\nabla_h \cdot \left(g\nabla_h \phi\right)_{i,j,k} = d_x \left(g_{\text{ew}} D_x \phi\right)_{i,j,k} + d_y \left(g_{\text{ns}} D_y \phi\right)_{i,j,k} + d_z \left(g_{\text{ud}} D_z \phi\right)_{i,j,k}, \tag{2.2}$$

in which the east-west, north-south, and up-down averages have been taken in the evaluation of g_{ew}, g_{ns} and g_{ud}, respectively. In the simple case that $g \equiv 1$, we write

$$\nabla_h \cdot \left(1\nabla_h \phi\right)_{i,j,k} = \Delta_h \phi_{i,j,k} = \nabla_h \cdot \left(\nabla_h \phi\right)_{i,j,k} = d_x \left(D_x \phi\right)_{i,j,k} + d_y \left(D_y \phi\right)_{i,j,k} + d_z \left(D_z \phi\right)_{i,j,k}. \tag{2.3}$$

For two cell-centered grid functions f and g, the discrete L^2_h inner product and the associated L^2_h norm are defined as

$$\langle f, g \rangle_\Omega := h^3 \sum_{i,j,k=1}^{N} f_{i,j,k} g_{i,j,k}, \quad \|f\|_2 := \sqrt{\langle f, f \rangle_\Omega}.$$

The mean zero space is introduced as

$$\mathring{\mathcal{C}}_{\text{per}} := \left\{ f \in \mathcal{C}_{\text{per}} \;\middle|\; 0 = \overline{f} := \frac{h^3}{|\Omega|} \sum_{i,j,k=1}^{m} f_{i,j,k} \right\}.$$

For any two vector grid functions $\vec{f} = (f^x, f^y, f^z)^T$, $\vec{g} = (g^x, g^y, g^z)^T \in \vec{\mathcal{E}}_{\text{per}}$ the corresponding discrete inner product becomes

$$\left[\vec{f}, \vec{g}\right]_\Omega := [f^x, g^x]_{\text{x}} + [g^y, g^y]_{\text{y}} + [f^z, g^z]_{\text{z}},$$

where

$$[f^x,g^x]_{\mathrm{x}}:=\langle a_x(f^xg^x),1\rangle_\Omega,\quad [f^y,g^y]_{\mathrm{y}}:=\langle a_y(f^yg^y),1\rangle_\Omega,\quad [f^z,g^z]_{\mathrm{z}}:=\langle a_z(f^zg^z),1\rangle_\Omega.$$

In addition to the discrete $\|\cdot\|_2$ norm, the discrete maximum norm is defined as $\|f\|_\infty:=\max_{1\le i,j,k\le N}|f_{i,j,k}|$. Moreover, the discrete H_h^1 norm is introduced as

$$\begin{aligned}&\|\nabla_h f\|_2^2:=[\nabla_h f,\nabla_h f]_\Omega=[D_x f,D_x f]_{\mathrm{x}}+\left[D_y f,D_y f\right]_{\mathrm{y}}+[D_z f,D_z f]_{\mathrm{z}},\\&\|f\|_{H_h^1}^2:=\|f\|_2^2+\|\nabla_h f\|_2^2.\end{aligned}\tag{2.4}$$

The following summation by parts formulas are recalled in the following lemma; the detailed proofs could be found in [37, 60, 62, 63], et cetera.

Lemma 2.1. [37, 60, 62, 63] *Suppose that g is an arbitrary Ω-periodic scalar function defined at all three face centers, and $\psi,\phi\in\mathcal{C}_{\mathrm{per}}$, and $\vec{f}=(f^x,f^y,f^z)^T\in\vec{\mathcal{E}}_{\mathrm{per}}$ are arbitrary. The following summation by parts formulas are valid:*

$$\left\langle\psi,\nabla_h\cdot\vec{f}\right\rangle_\Omega=-\left[\nabla_h\psi,\vec{f}\right]_\Omega,\quad \langle\psi,\nabla_h\cdot(g\nabla_h\phi)\rangle_\Omega=-[\nabla_h\psi,g\nabla_h\phi]_\Omega,\tag{2.5}$$

where

$$g\nabla_h\phi=\left(g_{\mathrm{ew}}D_x\phi,g_{\mathrm{ns}}D_y\phi,g_{\mathrm{ud}}D_z\phi\right)^T\in\vec{\mathcal{E}}_{\mathrm{per}}.$$

In addition, a discrete version of the space $H_{\mathrm{per}}^{-1}(\Omega)$ is needed to facilitate the analysis in the later sections. Suppose that g is a point-wise positive Ω-periodic scalar function defined at all three face centers. For any $\phi\in\mathcal{C}_{\mathrm{per}}$, it is clear that there is a unique $\psi\in\mathring{\mathcal{C}}_{\mathrm{per}}$ to the following discrete elliptic equation

$$\mathcal{L}_g(\psi):=-\nabla_h\cdot(g\nabla_h\psi)=\phi-\overline{\phi},\quad \overline{\phi}:=|\Omega|^{-1}\langle\phi,1\rangle_\Omega.\tag{2.6}$$

In turn, a bilinear form becomes available for this space:

$$\langle\phi_1,\phi_2\rangle_{\mathcal{L}_g^{-1}}:=[g\nabla_h\psi_1,\nabla_h\psi_2]_\Omega,\quad\forall\ \phi_1,\phi_2\in\mathring{\mathcal{C}}_{\mathrm{per}},$$

where

$$\mathcal{L}_g(\psi_i):=-\nabla_h\cdot(g\nabla_h\psi_i)=\phi_i,\quad i=1,2.$$

In turn, the following summation-by-parts identity is valid; see the proof in [60]:

$$\langle\phi_1,\phi_2\rangle_{\mathcal{L}_g^{-1}}=\left\langle\phi_1,\mathcal{L}_g^{-1}(\phi_2)\right\rangle_\Omega=\left\langle\mathcal{L}_g^{-1}(\phi_1),\phi_2\right\rangle_\Omega.\tag{2.7}$$

It is obvious that $\mathcal{L}_g$ is symmetric positive definite, so that $\langle\,\cdot\,,\,\cdot\,\rangle_{\mathcal{L}_g^{-1}}$ becomes an inner product on $\mathring{\mathcal{C}}_{\mathrm{per}}$.

In the trivial case $g\equiv1$, we use the notation $\mathcal{L}_1=-\Delta_h$, and $\langle\,\cdot\,,\,\cdot\,\rangle_{\mathcal{L}_g^{-1}}=\langle\,\cdot\,,\,\cdot\,\rangle_{-1,h}$. For a more general g, the norm associated to this inner product is defined as $\|\phi\|_{\mathcal{L}_g^{-1}}:=$

$\sqrt{\langle\phi,\phi\rangle_{\mathcal{L}_g^{-1}}}$, for any $\phi\in\mathring{\mathcal{C}}_{\rm per}$. Again, in the trivial case $g\equiv 1$, the corresponding norm is denoted as $\|\cdot\|_{\mathcal{L}_g^{-1}}=:\|\cdot\|_{-1,h}$.

The following estimate is needed in the later analysis; its proof has been provided in a recent work [13].

Lemma 2.2. [13] *Suppose that ϕ_1, $\phi_2\in\mathcal{C}_{\rm per}$, with $\langle\phi_1-\phi_2,1\rangle_\Omega=0$, that is, $\phi_1-\phi_2\in\mathring{\mathcal{C}}_{\rm per}$, and assume that $\|\phi_1\|_\infty,\|\phi_2\|_\infty<1$. Suppose that g is a point-wise positive Ω-periodic scalar function defined at all three face centers and $g\geq\mathcal{M}_0$. Then the following estimate is available:*

$$\|\mathcal{L}_g^{-1}(\phi_1-\phi_2)\|_\infty\leq C_2:=C_1\mathcal{M}_0^{-1}h^{-1/2},\tag{2.8}$$

where $C_1>0$ depends only upon Ω.

2.2 The numerical scheme and the theoretical result

The following second order accurate, fully discrete scheme is proposed: given $\phi^n,\phi^{n-1}\in\mathcal{C}_{\rm per}$, find $\phi^{n+1},\mu^{n+1/2}\in\mathcal{C}_{\rm per}$, such that

$$\frac{\phi^{n+1}-\phi^n}{\Delta t}=\nabla_h\cdot(\check{\mathcal{M}}^{n+1/2}\nabla_h\mu^{n+1/2}),\tag{2.9}$$

$$\begin{aligned}\mu^{n+1/2}=&\frac{F(1+\phi^{n+1})-F(1+\phi^n)}{\phi^{n+1}-\phi^n}+\frac{F(1-\phi^{n+1})-F(1-\phi^n)}{\phi^{n+1}-\phi^n}-\theta_0\check{\phi}^{n+1/2}-\varepsilon^2\Delta_h\hat{\phi}^{n+1/2}\\&+\Delta t(\ln(1+\phi^{n+1})-\ln(1+\phi^n)-\ln(1-\phi^{n+1})+\ln(1-\phi^n)),\end{aligned}\tag{2.10}$$

$$\check{\phi}^{n+1/2}:=\frac{3}{2}\phi^n-\frac{1}{2}\phi^{n-1},\quad\hat{\phi}^{n+1/2}:=\frac{3}{4}\phi^{n+1}+\frac{1}{4}\phi^{n-1},$$

where $F(x)=:x\ln x$. Observe that,

$$\frac{F(1\pm\phi(t_{n+1}))-F(1\pm\phi(t_n))}{\phi(t_{n+1})-\phi(t_n)}=\pm\ln(1\pm\phi(t_{n+1/2}))\pm1+\mathcal{O}(\Delta t^2).$$

The face-centered numerical mobility, $\check{\mathcal{M}}^{n+1/2}$, is defined by the following formulas:

$$\begin{aligned}\check{\mathcal{M}}^{n+1/2}_{i+1/2,j,k}&=\left(\mathcal{M}^2(A_x\check{\phi}^{n+1/2}_{i+1/2,j,k})+\Delta t^6\right)^{1/2},\\\check{\mathcal{M}}^{n+1/2}_{i,j+1/2,k}&=\left(\mathcal{M}^2(A_y\check{\phi}^{n+1/2}_{i,j+1/2,k})+\Delta t^6\right)^{1/2},\\\check{\mathcal{M}}^{n+1/2}_{i,j,k+1/2}&=\left(\mathcal{M}^2(A_z\check{\phi}^{n+1/2}_{i,j,k+1/2})+\Delta t^6\right)^{1/2}.\end{aligned}\tag{2.11}$$

This definition ensures both the second order temporal accuracy and a point-wise positive lower bound, $\check{\mathcal{M}}^{n+1/2}\geq\Delta t^3$, at every face center point.

We will prove in Theorem 3.1 that there exists a unique numerical solution for (2.9) - (2.10), as well as a point-wise bound for the grid function ϕ^{n+1}, namely, $-1<\phi^{n+1}_{i,j,k}<1$. As

a result, the numerical scheme is well-defined. To facilitate the theoretical analyses, the following three smooth functions are introduced: for any fixed $a>0$,

$$\begin{aligned} G_a^1(x) &:= \frac{F(x)-F(a)}{x-a}, \quad \forall x>0, \\ G_a^0(x) &:= \int_a^x G_a^1(t)dt = \int_a^x \frac{F(t)-F(a)}{t-a}dt, \quad \forall x>0, \\ G_a^2(x) &:= (G_a^1)'(x) = \frac{F'(x)(x-a)-(F(x)-F(a))}{(x-a)^2} = (G_a^0)''(x), \quad \forall x>0. \end{aligned} \tag{2.12}$$

The following preliminary estimates will be used in the later analysis. Their proofs are based on direct calculations, and the details are left to interested readers.

Lemma 2.3. *Let $a>0$ be fixed.*

1. *$G_a^2(x)\geq 0$, for any $x>0$.*
2. *$G_a^0(x)$ is convex, as a function of x, for $x>0$.*
3. *$(G_a^1)'(x)=\frac{1}{2\xi}$, for some ξ between a and x.*
4. *$G_a^1(x)$ is an increasing function of x, and $G_a^1(x)\leq G_a^1(a)=\ln a+1$ for any $0<x\leq a$.*

Remark 2.1. Since the proposed numerical scheme (2.9)-(2.10) is a three-level algorithm, a "ghost" point approximation for the phase variable value at t^{-1} is needed in the initialization process. For the sake of numerical convenience, a simple extrapolation formula $\phi^{-1}=\phi^0$ could be taken. Such a choice would simplify the energy stability analysis, and the overall second order numerical accuracy will also be preserved, due to the denominator fact Δt on the left hand side of the Crank-Nicolson method (2.9).

3 The positivity analysis

We will always assume that $-1<\phi^0<1$. Thus $|\overline{\phi_0}|<1$. It is observed that the numerical solution of (2.9) - (2.10) is mass conservative at a discrete level:

$$\overline{\phi^{n+1}}=\overline{\phi^n}=\cdots=\overline{\phi_0}, \quad \forall n\in\mathbb{N}. \tag{3.1}$$

Theorem 3.1. *Given $\phi^n,\phi^{n-1}\in\mathcal{C}_{\rm per}$, with $-1<\phi^n,\phi^{n-1}<1$, at a point-wise level. There exists a unique solution $\phi^{n+1}\in\mathcal{C}_{\rm per}$ to* (2.9)-(2.10)*, with $\phi^{n+1}-\overline{\phi^n}\in\mathring{\mathcal{C}}_{\rm per}$ and $\|\phi^{n+1}\|_\infty<1$.*

Proof. Since $\|\phi^n\|_\infty<1$, and there are finite number of grid points, we assume that

$$-1+\delta_0\leq\phi_{i,j,k}^n\leq 1-\delta_0, \quad \forall 1\leq i,j,k\leq N, \tag{3.2}$$

for some δ_0 that may depend upon t_n. The numerical solution of (2.9) is a minimizer of the following discrete energy functional:

$$\begin{aligned}\mathcal{J}^n(\phi):=&\frac{1}{2\Delta t}\|\phi-\phi^n\|^2_{\mathcal{L}^{-1}_{\check{\mathcal{M}}^{n+1/2}}}+\Delta t(\langle 1+\phi,\ln(1+\phi)\rangle_\Omega+\langle 1-\phi,\ln(1-\phi)\rangle_\Omega)\\&+\left\langle G^0_{1+\phi^n}(1+\phi),\mathbf{1}\right\rangle_\Omega-\left\langle G^0_{1-\phi^n}(1-\phi),\mathbf{1}\right\rangle_\Omega+\frac{3\varepsilon^2}{8}\|\nabla_h\phi\|_2^2+\langle\phi,f^n\rangle_\Omega,\end{aligned}\tag{3.3}$$

$$f^n:=-\theta_0\check{\phi}^{n+1/2}-\frac{1}{4}\varepsilon^2\Delta_h\phi^{n-1}+\Delta t(-\ln(1+\phi^n)+\ln(1-\phi^n)),\tag{3.4}$$

over an admissible set

$$A_h:=\left\{\phi\in\mathcal{C}_{\rm per}\;\middle|\;\|\phi\|_\infty\le 1,\ \langle\phi-\overline{\phi}_0,1\rangle_\Omega=0\right\}\subset\mathbb{R}^{N^3}.$$

It is clear that $\mathcal{J}^n$ is a strictly convex function over this domain. Meanwhile, we transform the minimization problem into an equivalent one, to facilitate later analysis:

$$\begin{aligned}\mathcal{F}^n(\varphi):=&\mathcal{J}^n(\varphi+\overline{\phi}_0)\\=&\frac{1}{2\Delta t}\|\varphi+\overline{\phi}_0-\phi^n\|^2_{\mathcal{L}^{-1}_{\check{\mathcal{M}}^{n+1/2}}}+\frac{3\varepsilon^2}{8}\|\nabla_h\varphi\|_2^2\\&+\Delta t(\langle 1+\varphi+\overline{\phi}_0,\ln(1+\varphi+\overline{\phi}_0)\rangle_\Omega+\langle 1-\varphi-\overline{\phi}_0,\ln(1-\varphi-\overline{\phi}_0)\rangle_\Omega)\\&+\left\langle G^0_{1+\phi^n}(1+\varphi+\overline{\phi}_0),\mathbf{1}\right\rangle_\Omega-\left\langle G^0_{1-\phi^n}(1-\varphi-\overline{\phi}_0),\mathbf{1}\right\rangle_\Omega+\langle\varphi+\overline{\phi}_0,f^n\rangle_\Omega,\end{aligned}\tag{3.5}$$

defined on the admissible set

$$\mathring{A}_h:=\left\{\varphi\in\mathring{\mathcal{C}}_{\rm per}\;\middle|\;-1-\overline{\phi}_0\le\varphi\le 1-\overline{\phi}_0\right\}\subset\mathbb{R}^{N^3}.$$

A minimizer $\varphi\in\mathring{A}_h$ of $\mathcal{F}^n$ is equivalent to the minimizer of $\phi:=\varphi+\overline{\phi}_0\in A_h$ for $\mathcal{J}^n$. Next, we aim to prove that there exists a minimizer of $\mathcal{F}^n$ over the domain $\mathring{A}_h$. For a sufficiently small δ, the following set is introduced

$$\mathring{A}_{h,\delta}:=\left\{\varphi\in\mathring{\mathcal{C}}_{\rm per}\;\middle|\;\delta-1-\overline{\phi}_0\le\varphi\le 1-\delta-\overline{\phi}_0\right\}\subset\mathbb{R}^{N^3}.\tag{3.6}$$

Since $\mathring{A}_{h,\delta}$ is a bounded, compact, and convex set in the subspace $\mathring{\mathcal{C}}_{\rm per}$, there exists a (not necessarily unique) minimizer of $\mathcal{F}^n$ over $\mathring{A}_{h,\delta}$. The key point of the positivity analysis is that such a minimizer could not occur on the boundary of $\mathring{A}_{h,\delta}$, if δ is sufficiently small. In fact, the boundary of $\mathring{A}_{h,\delta}$ refers to $\psi\in\mathring{A}_{h,\delta}$ with $\|\psi+\overline{\phi}_0\|_\infty=1-\delta$.

We aim to derive a contradiction. Suppose that the minimizer $\varphi^\star$ of $\mathcal{F}^n$ occurs at a boundary point of $\mathring{A}_{h,\delta}$. In turn, there is at least one grid point $\vec{\alpha}_0=(i_0,j_0,k_0)$ with $|\varphi^\star_{\vec{\alpha}_0}+\overline{\phi}_0|=1-\delta$. Without loss of generality, it is assumed that $\varphi^\star_{\vec{\alpha}_0}+\overline{\phi}_0=\delta-1$, so that the grid function $\varphi^\star$ has a global minimum at $\vec{\alpha}_0$. We also assume that $\vec{\alpha}_1=(i_1,j_1,k_1)$ is a grid

point at which $\varphi^\star$ achieves its maximum. On the other hand, the identity $\overline{\varphi^\star}=0$ implies that

$$1-\delta\geq\varphi^\star_{\vec{\alpha}_1}+\overline{\phi}_0\geq\overline{\phi}_0.$$

Meanwhile, since $\mathcal{F}^n$ is smooth over $\mathring{A}_{h,\delta}$, the directional derivative is calculated as

$$\begin{aligned}d_s\mathcal{F}^n(\varphi^\star+s\psi)|_{s=0}=&\Delta t\big\langle\ln(1+\varphi^\star+\overline{\phi}_0)-\ln(1-\varphi^\star-\overline{\phi}_0),\psi\big\rangle_\Omega\\&+\Big\langle G^1_{1+\phi^n}(1+\varphi+\overline{\phi}_0)-G^1_{1-\phi^n}(1-\varphi-\overline{\phi}_0),\psi\Big\rangle_\Omega\\&+\langle f^n-\frac{3}{4}\varepsilon^2\Delta_h\varphi^\star,\psi\rangle_\Omega+\frac{1}{\Delta t}\langle\mathcal{L}^{-1}_{\check{\mathcal{M}}^{n+1/2}}(\varphi^\star-\phi^n+\overline{\phi}_0),\psi\rangle_\Omega.\end{aligned}$$

Let $\delta_{i,j}$ denote the Kronecker delta function. We choose the direction $\psi\in\mathring{\mathcal{C}}_{\rm per}$ with $\psi_{i,j,k}=\delta_{i,i_0}\delta_{j,j_0}\delta_{k,k_0}-\delta_{i,i_1}\delta_{j,j_1}\delta_{k,k_1}$. Then the derivative becomes

$$\begin{aligned}\frac{1}{h^3}d_s\mathcal{F}^n(\varphi^\star+s\psi)|_{s=0}=&\Delta t(\ln(1+\varphi^\star_{\vec{\alpha}_0}+\overline{\phi}_0)-\ln(1-\varphi^\star_{\vec{\alpha}_0}-\overline{\phi}_0)\\&-\ln(1+\varphi^\star_{\vec{\alpha}_1}+\overline{\phi}_0)+\ln(1-\varphi^\star_{\vec{\alpha}_1}-\overline{\phi}_0))\\&+G^1_{1+\phi^n}(1+\varphi^\star_{\vec{\alpha}_0}+\overline{\phi}_0)-G^1_{1-\phi^n}(1-\varphi^\star_{\vec{\alpha}_0}-\overline{\phi}_0)\\&-G^1_{1+\phi^n}(1+\varphi^\star_{\vec{\alpha}_1}+\overline{\phi}_0)+G^1_{1-\phi^n}(1-\varphi^\star_{\vec{\alpha}_1}-\overline{\phi}_0)\\&+(f^n_{\vec{\alpha}_0}-f^n_{\vec{\alpha}_1})-\frac{3}{4}\varepsilon^2(\Delta_h\varphi^\star_{\vec{\alpha}_0}-\Delta_h\varphi^\star_{\vec{\alpha}_1})\\&+\frac{1}{\Delta t}(\mathcal{L}^{-1}_{\check{\mathcal{M}}^{n+1/2}}(\varphi^\star-\phi^n+\overline{\phi}_0)_{\vec{\alpha}_0}-\mathcal{L}^{-1}_{\check{\mathcal{M}}^{n+1/2}}(\varphi^\star-\phi^n+\overline{\phi}_0)_{\vec{\alpha}_1}).\end{aligned}\tag{3.7}$$

For simplicity, we rewrite $\phi^\star:=\varphi^\star+\overline{\phi}_0$. Since $\phi^\star_{\vec{\alpha}_0}=-1+\delta$ and $\phi^\star_{\vec{\alpha}_1}\geq\overline{\phi}_0$, the following inequality is valid:

$$\ln(1+\phi^\star_{\vec{\alpha}_0})-\ln(1-\phi^\star_{\vec{\alpha}_0})-\ln(1+\phi^\star_{\vec{\alpha}_1})+\ln(1-\phi^\star_{\vec{\alpha}_1})\leq\ln\frac{\delta}{2-\delta}-\ln\frac{1+\overline{\phi}_0}{1-\overline{\phi}_0}.\tag{3.8}$$

Similarly, since $G^1_a(x)$ is an increasing function in terms of x (for a fixed $a>0$), as given by Lemma 2.3, the following inequalities could be derived:

$$\begin{aligned}&G^1_{1+\phi^n}(1+\phi^\star_{\vec{\alpha}_0})=G^1_{1+\phi^n}(\delta)\leq G^1_{1+\phi^n}(1+\phi^n)=\ln(1+\phi^n)+1,\\&G^1_{1-\phi^n}(1-\phi^\star_{\vec{\alpha}_0})=G^1_{1-\phi^n}(2-\delta)\geq G^1_{1-\phi^n}(1),\\&G^1_{1+\phi^n}(1+\phi^\star_{\vec{\alpha}_1})\geq G^1_{1+\phi^n}(1+\overline{\phi}_0),\\&G^1_{1-\phi^n}(1-\phi^\star_{\vec{\alpha}_1})\leq G^1_{1-\phi^n}(1-\overline{\phi}_0).\end{aligned}\tag{3.9}$$

Since $\phi^\star$ takes a minimum at the grid point $\vec{\alpha}_0$ and a maximum at the grid point $\vec{\alpha}_1$, we see that $\phi^\star_{\vec{\alpha}_0}=-1+\delta\leq\phi^\star_{i,j,k}$, and $\phi^\star_{\vec{\alpha}_1}\geq\phi^\star_{i,j,k}$, for any (i,j,k). This fact indicates that

$$\Delta_h\phi^\star_{\vec{\alpha}_0}\geq0,\quad\Delta_h\phi^\star_{\vec{\alpha}_1}\leq0.\tag{3.10}$$

For the force term f^n at the previous time steps, the condition $\|\phi^n\|_\infty, \|\phi^{n-1}\|_\infty < 1$, combined with the refined bound (3.2), indicates that

$$\begin{aligned} |f^n| &\le \theta_0 |\check{\phi}^{n+1/2}| + \frac{1}{4}\varepsilon^2 |\Delta_h \phi^{n-1}| + \Delta t (|\ln(1+\phi^n)| + |\ln(1-\phi^n)|) \\ &\le 2\theta_0 + \frac{1}{4}\varepsilon^2 \cdot \frac{12}{h^2} + 2\Delta t |\ln \delta_0| \\ &= 2\theta_0 + 3\varepsilon^2 h^{-2} + 2\Delta t |\ln \delta_0|, \end{aligned} \tag{3.11}$$

at a point-wise level. This in turn implies that

$$-4\theta_0 - 6\varepsilon^2 h^{-2} - 4\Delta t |\ln \delta_0| \le f^n_{\vec{\alpha}_0} - f^n_{\vec{\alpha}_1} \le 4\theta_0 + 6\varepsilon^2 h^{-2} + 4\Delta t |\ln \delta_0|. \tag{3.12}$$

For the last two terms appearing in (3.7), we apply Lemma 2.2 to obtain (keeping in mind that $\phi^* = \varphi^* + \bar{\phi}_0$)

$$-2C_2 \le \mathcal{L}^{-1}_{\check{\mathcal{M}}^{n+1/2}} (\phi^\star - \phi^n)_{\vec{\alpha}_0} - \mathcal{L}^{-1}_{\check{\mathcal{M}}^{n+1/2}} (\phi^\star - \phi^n)_{\vec{\alpha}_1} \le 2C_2. \tag{3.13}$$

Notice that C_2 has a singular dependence on Δt and h, due to the representation formula (2.8) and the fact that $\mathcal{M}_0 = \Delta t^3$. As a consequence, a substitution of (3.8) – (3.13) into (3.7) yields the following bound on the directional derivative:

$$\begin{aligned} \frac{1}{h^3} d_s \mathcal{F}^n(\varphi^\star + s\psi)|_{s=0} \le & \Delta t \left(\ln \frac{\delta}{2-\delta} - \ln \frac{1+\overline{\phi}_0}{1-\overline{\phi}_0} \right) + 4\theta_0 + 6\varepsilon^2 h^{-2} + 4\Delta t |\ln \delta_0| + 2C_2 \Delta t^{-1} \\ & + \ln(1+\phi^n) + 1 - G^1_{1-\phi^n}(1) - G^1_{1+\phi^n}(1+\overline{\phi}_0) + G^1_{1-\phi^n}(1-\overline{\phi}_0). \end{aligned} \tag{3.14}$$

In turn, we define

$$\begin{aligned} D_0 := & 4\theta_0 + 6\varepsilon^2 h^{-2} + 4\Delta t |\ln \delta_0| + 2C_2 \Delta t^{-1} + \ln(1+\phi^n) + 1 \\ & - G^1_{1-\phi^n}(1) - G^1_{1+\phi^n}(1+\overline{\phi}_0) + G^1_{1-\phi^n}(1-\overline{\phi}_0), \end{aligned}$$

a constant that will, in general, depend upon Δt, h, δ_0 and $\overline{\phi}_0$. The parameter δ can be chosen sufficiently small so that

$$\Delta t \left(\ln \frac{\delta}{2-\delta} - \ln \frac{1+\overline{\phi}_0}{1-\overline{\phi}_0} \right) + D_0 < 0. \tag{3.15}$$

Therefore, the following inequality becomes available

$$\frac{1}{h^3} d_s \mathcal{F}^n(\varphi^\star + s\psi)|_{s=0} < 0, \tag{3.16}$$

provided that δ satisfies (3.15). This inequality clearly contradicts the assumption that $\mathcal{F}^n$ has a minimum at $\varphi^\star$, due to the fact that the directional derivative is negative in a direction pointing into the interior of $\mathring{A}_{h,\delta}$.

Using analogous estimates, we can also prove that, similarly, the global minimum of $\mathcal{F}^n$ over $\mathring{A}_{h,\delta}$ could not occur at a boundary point $\varphi^\star$ such that $\varphi^\star_{\vec{\alpha}_0}+\overline{\phi}_0=1-\delta$, for some $\vec{\alpha}_0$. The analysis could be derived in a similar fashion and the details are left to interested readers.

A combination of these two facts reveals that, the global minimum of $\mathcal{F}^n$ over $\mathring{A}_{h,\delta}$ could only possibly occur at interior point $\varphi\in(\mathring{A}_{h,\delta})^{\rm o}\subset(\mathring{A}_h)^{\rm o}$. As a result, there must be a solution $\phi=\varphi+\overline{\phi}_0\in A_h$ that minimizes $\mathcal{J}^n$ over A_h, which is equivalent to the numerical solution of (2.9), (2.10). The existence of the numerical solution is confirmed.

Furthermore, because of the strict convexity of $\mathcal{J}^n$ over A_h, the uniqueness analysis for this numerical solution is straightforward. This completes the proof of Theorem 3.1. □

Remark 3.1. The modified Crank-Nicolson approximation to the nonlinear logarithmic terms, namely $G^1_{1+\phi^n}(1+\phi^{n+1})-G^1_{1-\phi^n}(1-\phi^{n+1})$, makes its inner product with $\phi^{n+1}-\phi^n$ exactly the difference of the logarithmic energies between two consecutive time steps. This fact will greatly facilitate the energy stability analysis, as we will see in the next section. Meanwhile, it is observed that, the proposed nonlinear approximation terms, $G^1_{1+\phi^n}(1+\phi^{n+1})$ and $-G^1_{1-\phi^n}(1-\phi^{n+1})$, do not indicate a singularity as $\phi^{n+1}\to-1$ or 1, respectively. Such a feature leads to a difficulty of a theoretical justification for the positivity-preserving property. To overcome this difficulty, a nonlinear regularization term, in the form of $\Delta t(\ln(1\pm\phi^{n+1})-\ln(1\pm\phi^n))$, is added in the numerical scheme. Although this artificial regularization term is of order $O(\Delta t^2)$, a singularity becomes available as $\phi^{n+1}\to-1$ or 1. This singularity plays and important role in the theoretical justification of the positivity-preserving property for the proposed numerical scheme (2.9).

Remark 3.2. It is observed that, a point-wise positivity of the numerical mobility function, namely, $\check{\mathcal{M}}^{n+1/2}>0$, is needed to ensure the elliptic operator nature of $\mathcal{L}^{-1}_{\check{\mathcal{M}}^{n+1/2}}(\phi^\star-\phi^n)$, so that the estimate (3.13) becomes valid. If a zero value is reached for the numerical value of $\check{\mathcal{M}}^{n+1/2}$ at a numerical grid point, the theoretical analysis would face certain difficulty. On the other hand, there are some physical examples with a possible degenerate mobility function, such as $\mathcal{M}(\phi)=\gamma(1+\phi)(1-\phi)$. In fact, this difficulty could be overcome in the numerical design, such as the positivity-regularization formula (2.11), in which both the second order numerical accuracy and a point-wise positivity of the mobility function have been preserved, even if the mobility function may be degenerate.

4 Energy stability estimate and uniform in time H^1_h bound

The discrete energy is defined as follows: for any $\phi\in\mathcal{C}_{\rm per}$, $-1\le\phi\le1$,

$$E_h(\phi):=\langle1+\phi,\ln(1+\phi)\rangle_\Omega+\langle1-\phi,\ln(1-\phi)\rangle_\Omega+\frac{\varepsilon^2}{2}\|\nabla_h\phi\|_2^2-\frac{\theta_0}{2}\|\phi\|_2^2. \tag{4.1}$$

We also defined a modified energy via

$$\tilde{E}_h(\phi,\psi):=E_h(\phi)+\frac{1}{4}\|\phi-\psi\|_2^2+\frac{\varepsilon^2}{8}\|\nabla_h(\phi-\psi)\|_2^2, \tag{4.2}$$

for any $\phi\in\mathcal{C}_{\rm per}$, with $-1\leq\phi,\leq 1$ and any $\psi\in\mathcal{C}_{\rm per}$. A modified energy stability is stated in the following theorem.

Theorem 4.1. *For the unique numerical solution of* (2.9)-(2.10)*, the following dissipation property is valid:*

$$\tilde{E}_h(\phi^{n+1},\phi^n)\leq\tilde{E}_h(\phi^n,\phi^{n-1}). \tag{4.3}$$

Thus, for any $m\geq 0$*,*

$$E_h(\phi^m)\leq\tilde{E}_h(\phi^m,\phi^{m-1})\leq\cdots\leq\tilde{E}_h(\phi^1,\phi^0)\leq\tilde{E}_h(\phi^0,\phi^{-1})=E_h(\phi^0)\leq C_3,$$

where $C_3>0$ *is independent of* h*, if we take* $\phi^{-1}=\phi^0$*. In addition, since*

$$-\frac{\theta_0}{2}|\Omega|+\frac{\varepsilon^2}{2}\|\nabla_h\phi^m\|_2^2\leq E_h(\phi^m),$$

it follows that

$$\|\nabla_h\phi^m\|_2\leq\frac{\sqrt{2C_3+\theta_0|\Omega|}}{\varepsilon}=:C_4,\quad\forall m\in\mathbb{N}. \tag{4.4}$$

Proof. Taking a discrete inner product of (2.9) with $\mu^{n+1/2}$ leads to

$$\langle\phi^{n+1}-\phi^n,\mu^{n+1/2}\rangle_\Omega+\left[\check{\mathcal{M}}^{n+1/2}\nabla_h\mu^{n+1/2},\nabla_h\mu^{n+1/2}\right]_\Omega=0. \tag{4.5}$$

In the expansion of $\langle\phi^{n+1}-\phi^n,\mu^{n+1/2}\rangle_\Omega$, the following equalities and inequalities are available for the inner products associated with the nonlinear logarithmic terms:

$$\begin{aligned}
I_1:&=\left\langle\phi^{n+1}-\phi^n,\frac{F(1+\phi^{n+1})-F(1+\phi^n)}{\phi^{n+1}-\phi^n}\right\rangle_\Omega\\
&=\left\langle 1+\phi^{n+1},\ln(1+\phi^{n+1})\right\rangle_\Omega-\langle 1+\phi^n,\ln(1+\phi^n)\rangle_\Omega, &(4.6)\\
I_2:&=\left\langle\phi^{n+1}-\phi^n,\frac{F(1-\phi^{n+1})-F(1-\phi^n)}{\phi^{n+1}-\phi^n}\right\rangle_\Omega\\
&=\left\langle 1-\phi^{n+1},\ln(1-\phi^{n+1})\right\rangle_\Omega-\langle 1-\phi^n,\ln(1-\phi^n)\rangle_\Omega, &(4.7)\\
I_3:&=\langle\phi^{n+1}-\phi^n,\ln(1+\phi^{n+1})-\ln(1+\phi^n)\rangle_\Omega\geq 0, &(4.8)\\
I_4:&=\langle\phi^{n+1}-\phi^n,-\ln(1-\phi^{n+1})+\ln(1-\phi^n)\rangle_\Omega\geq 0. &(4.9)
\end{aligned}$$

For the surface diffusion and expansive terms, the following estimates could be derived:

$$\begin{aligned}
I_5 :=& \Big\langle \phi^{n+1}-\phi^n, -\Delta_h\Big(\frac{3}{4}\phi^{n+1}+\frac{1}{4}\phi^{n-1}\Big)\Big\rangle_\Omega \\
=& \Big\langle \nabla_h(\phi^{n+1}-\phi^n), \nabla_h\Big(\frac{3}{4}\phi^{n+1}+\frac{1}{4}\phi^{n-1}\Big)\Big\rangle_\Omega \\
=& \frac{1}{2}\langle \nabla_h(\phi^{n+1}-\phi^n), \nabla_h(\phi^{n+1}+\phi^n)\rangle_\Omega + \frac{1}{4}\langle \nabla_h(\phi^{n+1}-\phi^n), \nabla_h(\phi^{n+1}-2\phi^n+\phi^{n-1})\rangle_\Omega \\
\geq& \frac{1}{2}(\|\nabla_h\phi^{n+1}\|_2^2 - \|\nabla_h\phi^n\|_2^2) + \frac{1}{8}(\|\nabla_h(\phi^{n+1}-\phi^n)\|_2^2 - \|\nabla_h(\phi^n-\phi^{n-1})\|_2^2), \qquad (4.10) \\
I_6 :=& \Big\langle \phi^{n+1}-\phi^n, -\frac{3}{2}\phi^n+\frac{1}{2}\phi^{n-1}\Big\rangle_\Omega \\
=& \langle \phi^{n+1}-\phi^n, -\phi^n\rangle_\Omega - \frac{1}{2}\langle \phi^{n+1}-\phi^n, \phi^n-\phi^{n-1}\rangle_\Omega \\
\geq& -\frac{1}{2}(\|\phi^{n+1}\|_2^2 - \|\phi^n\|_2^2) + \frac{1}{4}(\|\phi^{n+1}-\phi^n\|_2^2 - \|\phi^n-\phi^{n-1}\|_2^2). \qquad (4.11)
\end{aligned}$$

Finally, a substitution of (4.6)-(4.11) into (4.5) yields (4.3), so that the modified energy stability is proved.

The discrete H^1 estimate (4.4) comes from a direct energy inequality, $-\frac{\theta_0}{2}|\Omega| + \frac{\varepsilon^2}{2}\|\nabla_h\phi^m\|_2^2 \leq E_h(\phi^m)$, for any $m \geq 0$. The proof of Theorem 4.1 is complete. □

Remark 4.1. There have been very recent works that utilize explicit numerical approximations for the singular parts. In [45], a first order accurate numerical scheme is considered, with fully explicit approximation for the logarithmic terms. The energy stability of such a numerical scheme relies on a separation property of the numerical solution for the 2-D Cahn-Hilliard flow with Flory-Huggins energy (1.1), i.e., a uniform distance between the solution and the singular limit values of 1 and -1. In fact, such a separation property has been theoretically derived for the PDE solution [1, 4, 18, 28, 33, 34, 52].

The analysis in [45] turns out to be more involved than the present work. A time step constraint is needed to ensure the energy stability and the positivity property of the phase variables for this linear numerical scheme, and such a constraint depends on ε, θ_0, as well as the uniform distance between the PDE solution away from the singular limit values. For most practically interesting problems, such a uniform distance is quite small, which may lead to a severe time step constraint. In comparison, although the proposed numerical scheme (2.9), (2.10) is highly nonlinear, the positivity-preserving property and energy stability holds for any time-step size. Moreover, an efficient iteration solver will be introduced in the later sections, in which the computational cost is comparable to a few standard Poisson solvers, as demonstrated by extensive numerical experiments. As a result, both the theoretical properties and the efficiency/accuracy have been validated for the proposed second order scheme (2.9), (2.10) in this article.

Remark 4.2. The modified Crank-Nicolson approximation to the logarithmic nonlinear

term,

$$\frac{F(1\pm\phi^{n+1})-F(1\pm\phi^{n})}{\phi^{n+1}-\phi^{n}},$$

plays an essential role in the energy stability analysis. Such a modified Crank-Nicolson approximation has been successfully applied to various gradient flows, such as the polynomial approximation of the Cahn-Hilliard equation [10,17,21,22,37,38], phase field crystal [5,6,24,40], epitaxial thin film growth [12,59], nonlinear model [35,36], et cetera. Meanwhile, all these existing works have been focused on an energy potential well-defined over the whole space, while the proposed scheme (2.9) is the first work to theoretically justify the energy stability of a modified Crank-Nicolson method to a gradient flow with singular logarithmic energy potential.

Remark 4.3. Besides the Crank-Nicolson approach employed here, there have been a few recent works of the second order BDF schemes for certain gradient flow models, such as polynomial version of Cahn-Hilliard [14, 15, 48, 64], epitaxial thin film equation [32, 39, 46, 51], square phase field crystal [16], in which the energy stability was theoretically established. A successful extension to the Cahn-Hilliard equation with Flory-Huggins energy has also been reported in [13, 27].

Meanwhile, most of these BDF-type schemes are applied to constant-mobility gradient flows, while a theoretical justification of energy stability for the non-constant mobility case will face serious difficulty, due to the long-stencil temporal discretization involved. Some other high-order accurate and energy stable numerical approaches, such as the variational extrapolation method [67], have been primarily focused on the case of constant mobility and L^2 gradient flow structure, while an extension to an H^{-1} gradient flow with nonlinear mobility function is always a more challenging issue. In comparison, for the proposed scheme (2.9), both the positivity-preserving property and the energy stability could be theoretically justified, which comes from the modified Crank-Nicolson framework

5 Optimal rate convergence analysis

For simplicity of presentation, we assume a constant mobility, $\mathcal{M}\equiv 1$, in this section. The convergence analysis for the non-constant mobility flow is more complicated. But, it can be handled, with more technical detail, using the techniques developed for the Poisson-Nernst-Planck system [50].

Denote by Φ the exact solution for the Cahn-Hilliard flow (1.2)-(1.3). With sufficiently regular initial data, it is assumed that the exact solution has regularity of class $\mathcal{R}$:

$$\Phi\in\mathcal{R}:=H^3\left(0,T;C_{\rm per}(\Omega)\right)\cap H^2\left(0,T;C^2_{\rm per}(\Omega)\right)\cap L^\infty\left(0,T;C^6_{\rm per}(\Omega)\right). \tag{5.1}$$

In addition, we assume that the following separation property is valid for the exact solution:

$$1+\Phi\geq\epsilon_0,\quad 1-\Phi\geq\epsilon_0,\quad \text{at the point-wise level, for some } \epsilon_0>0. \tag{5.2}$$

Subsequently, we introduce $\Phi_N(\cdot,t):=\mathcal{P}_N\Phi(\cdot,t)$, the Fourier projection of the exact solution into $\mathcal{B}^K$, the space of trigonometric polynomials of degree to and including K. The following projection approximation is standard: for any $\Phi\in L^\infty(0,T;H^\ell_{\rm per}(\Omega))$, there is a constant, $C>0$, independent of N,

$$\|\Phi_N-\Phi\|_{L^\infty(0,T;H^k)}\le Ch^{\ell-k}\|\Phi\|_{L^\infty(0,T;H^\ell)},\quad \forall\, 0\le k\le \ell. \tag{5.3}$$

In fact, this Fourier projection estimate does not preserve the positivity of the variables. However, we could take h sufficiently small (that is, N sufficiently large) so that

$$1+\Phi_N,\, 1-\Phi_N\ge\frac{1}{2}\epsilon_0. \tag{5.4}$$

By Φ_N^m, Φ^m we denote $\Phi_N(\cdot,t_m)$ and $\Phi(\cdot,t_m)$, respectively, with $t_m=m\cdot\Delta t$. In turn, the mass conservative property is available at the discrete level, since $\Phi_N\in\mathcal{B}^K$:

$$\overline{\Phi_N^m}=\frac{1}{|\Omega|}\int_\Omega\Phi_N(\cdot,t_m)d\mathbf{x}=\frac{1}{|\Omega|}\int_\Omega\Phi_N(\cdot,t_{m-1})d\mathbf{x}=\overline{\Phi_N^{m-1}},\quad\forall\, m\in\mathbb{N}. \tag{5.5}$$

On the other hand, we notice that the numerical solution of (2.9), (2.10) is also mass conservative at a discrete level, as given by (3.1). For the initial data, we use

$$\phi^{-1}_{i,j,k}=\phi^0_{i,j,k}:=\Phi_N(p_i,p_j,p_k,t=0). \tag{5.6}$$

Since we use the Fourier projection, it follows that, for any $k\in\mathbb{N}$,

$$\left\langle\phi^k,1\right\rangle_\Omega=\cdots=\left\langle\phi^0,1\right\rangle_\Omega=(\Phi_N(\cdot,0),1)=(\Phi(\cdot,0),1)=\cdots=(\Phi(\cdot,t_k),1).$$

The error grid function is defined as

$$\tilde\phi^m:=\Phi_N^m-\phi^m,\quad\forall\, m\ge0. \tag{5.7}$$

As a result, it follows that $\overline{\tilde\phi^m}=0$, for any $m\ge0$, so that the discrete norm $\|\cdot\|_{-1,h}$ is well defined for the error grid function.

In fact, although the initialization (5.6) is only first order accurate for the phase variable at a "ghost" temporal instant t^{-1}, this approximation does not affect the overall second order accuracy in time. Since the Crank-Nicolson temporal stencil is only involved with ϕ^{n+1} and ϕ^n, we see that ϕ^{-1} does not enter into the temporal stencil in the first time step. Instead, it only enters into the numerical scheme as a right hand side force term. In turn, because of the Δt term on the denominator in the temporal stencil, the initial time step algorithm still gives an $\mathcal{O}(\Delta t^2)$ approximation to ϕ^1. Furthermore, since ϕ^1 is an $\mathcal{O}(\Delta t^2)$ approximation to Φ^1, the numerical scheme at the rest time steps corresponds to second order temporal truncation errors.

Theorem 5.1. *Given initial data $\Phi(\cdot,t=0)\in C^6_{\rm per}(\Omega)$, suppose the exact solution for Cahn-Hilliard equation* (1.2)-(1.3) *is of regularity class $\mathcal{R}$. Suppose that Δt and h are sufficiently small and satisfy the linear refinement condition $C_5h\le\Delta t\le C_6h$, for some $0<C_5\le C_6$. Then*

$$\|\tilde{\phi}^n\|_{-1,h}+\left(\varepsilon^2\Delta t\sum_{m=1}^{n}\|\nabla_h\tilde{\phi}^m\|_2^2\right)^{1/2}\le C(\Delta t^2+h^2), \tag{5.8}$$

for some constant $C>0$ that is independent of n, Δt, and h.

Proof. A careful consistency analysis reveals the following truncation error estimate:

$$\begin{aligned}\frac{\Phi_N^{n+1}-\Phi_N^n}{\Delta t}=\Delta_h\Bigg\{&\frac{F(1+\Phi_N^{n+1})-F(1+\Phi_N^n)}{\Phi_N^{n+1}-\Phi_N^n}+\frac{F(1-\Phi_N^{n+1})-F(1-\Phi_N^n)}{\Phi_N^{n+1}-\Phi_N^n}\\&+\Delta t(\ln(1+\Phi_N^{n+1})-\ln(1+\Phi_N^n)-\ln(1-\Phi_N^{n+1})+\ln(1-\Phi_N^n))\\&-\theta_0\left(\frac{3}{2}\Phi_N^n-\frac{1}{2}\Phi_N^{n-1}\right)-\varepsilon^2\Delta_h\left(\frac{3}{4}\Phi_N^{n+1}+\frac{1}{4}\Phi_N^{n-1}\right)\Bigg\}+\tau^n,\end{aligned} \tag{5.9}$$

with $\|\tau^n\|_{-1,h}\le C(\Delta t^2+h^2)$. Subtracting the numerical scheme (2.9) from (5.9) results in

$$\begin{aligned}\frac{\tilde{\phi}^{n+1}-\tilde{\phi}^n}{\Delta t}=\Delta_h\Bigg\{&(\mathcal{N}_1^n+\mathcal{N}_2^n+\Delta t(\mathcal{N}_3^n+\mathcal{N}_4^n+\mathcal{N}_5^n+\mathcal{N}_6^n)\\&-\theta_0\left(\frac{3}{2}\tilde{\phi}^n-\frac{1}{2}\tilde{\phi}^{n-1}\right)-\varepsilon^2\Delta_h\left(\frac{3}{4}\tilde{\phi}^{n+1}+\frac{1}{4}\tilde{\phi}^{n-1}\right)\Bigg\}+\tau^n,\end{aligned} \tag{5.10}$$

where

$$\begin{aligned}\mathcal{N}_1^n&:=\frac{F(1+\Phi_N^{n+1})-F(1+\Phi_N^n)}{\Phi_N^{n+1}-\Phi_N^n}-\frac{F(1+\phi^{n+1})-F(1+\phi^n)}{\phi^{n+1}-\phi^n},\\
\mathcal{N}_2^n&:=\frac{F(1-\Phi_N^{n+1})-F(1-\Phi_N^n)}{\Phi_N^{n+1}-\Phi_N^n}-\frac{F(1-\phi^{n+1})-F(1-\phi^n)}{\phi^{n+1}-\phi^n},\\
\mathcal{N}_3^n&:=\ln(1+\Phi_N^{n+1})-\ln(1+\phi^{n+1}),\\
\mathcal{N}_4^n&:=-\ln(1+\Phi_N^n)+\ln(1+\phi^n),\\
\mathcal{N}_5^n&:=-\ln(1-\Phi_N^{n+1})+\ln(1-\phi^{n+1}),\\
\mathcal{N}_6^n&:=\ln(1-\Phi_N^n)-\ln(1-\phi^n).\end{aligned}$$

To proceed with the nonlinear analysis, we make the following a-priori assumption at the previous time step:

$$\|\tilde{\phi}^n\|_2\le\Delta t^{\frac{13}{8}}+h^{\frac{13}{8}}. \tag{5.11}$$

Such an a-priori assumption will be recovered by the optimal rate convergence analysis at the next time step, as will be demonstrated later. In turn, a discrete $\|\cdot\|_\infty$ bound is available for the numerical error function at the previous time step, with the help of inverse inequality:

$$\|\tilde{\phi}^n\|_\infty \le \frac{C\|\tilde{\phi}^n\|_2}{h^{\frac{3}{2}}} \le \frac{C(\Delta t^{\frac{13}{8}}+h^{\frac{13}{8}})}{h^{\frac{3}{2}}} \le C(\Delta t^{\frac{1}{8}}+h^{\frac{1}{8}}) \le \frac{\epsilon_0}{4}, \tag{5.12}$$

provided that Δt and h are sufficiently small. Also notice that the linear refinement constraint $C_5 h \le \Delta t \le C_6 h$ has been used. In turn, the separation property is also valid for the numerical solution at the previous time step:

$$1+\phi^n \ge 1+\Phi_N^n - \|\tilde{\phi}^n\|_\infty \ge \frac{\epsilon_0}{4}, \quad 1-\phi^n \ge 1-\Phi_N^n - \|\tilde{\phi}^n\|_\infty \ge \frac{\epsilon_0}{4}, \tag{5.13}$$

where the separation estimate (5.4) has been utilized.

First, $(-\Delta_h)^{-1}\tilde{\phi}^m$ is well-defined for any $m \ge 0$, since $\tilde{\phi}^m$ has zero-mean. In turn, taking a discrete inner product with (5.10) by $2(-\Delta_h)^{-1}\tilde{\phi}^{n+1}$ gives

$$\begin{aligned}
&\frac{1}{\Delta t}\Big(\|\tilde{\phi}^{n+1}\|_{-1,h}^2 - \|\tilde{\phi}^n\|_{-1,h}^2 + \|\tilde{\phi}^{n+1}-\tilde{\phi}^n\|_{-1,h}^2\Big) \\
&\quad + \varepsilon^2\left\langle \nabla_h\tilde{\phi}^{n+1}, \nabla_h\left(\frac{3}{2}\tilde{\phi}^{n+1}+\frac{1}{2}\tilde{\phi}^{n-1}\right)\right\rangle_\Omega + 2\sum_{j=1}^{2}\langle \mathcal{N}_j^n, \tilde{\phi}^{n+1}\rangle_\Omega + 2\Delta t\sum_{j=3}^{6}\langle \mathcal{N}_j^n, \tilde{\phi}^{n+1}\rangle_\Omega \\
&= \theta_0\langle 3\tilde{\phi}^n - \tilde{\phi}^{n-1}, \tilde{\phi}^{n+1}\rangle_\Omega + 2\langle \tau^n, \tilde{\phi}^{n+1}\rangle_{-1,h}.
\end{aligned} \tag{5.14}$$

The estimate for the term associated with the surface diffusion could be carried out as follows:

$$\begin{aligned}
\left\langle \nabla_h\tilde{\phi}^{n+1}, \nabla_h\left(\frac{3}{2}\tilde{\phi}^{n+1}+\frac{1}{2}\tilde{\phi}^{n-1}\right)\right\rangle_\Omega &= \frac{3}{2}\|\nabla_h\tilde{\phi}^{n+1}\|_2^2 + \frac{1}{2}\langle \nabla_h\tilde{\phi}^{n+1}, \nabla_h\tilde{\phi}^{n-1}\rangle_\Omega \\
&\ge \frac{3}{2}\|\nabla_h\tilde{\phi}^{n+1}\|_2^2 - \frac{1}{4}(\|\nabla_h\tilde{\phi}^{n+1}\|_2^2 + \|\nabla_h\tilde{\phi}^{n-1}\|_2^2) \\
&= \frac{5}{4}\|\nabla_h\tilde{\phi}^{n+1}\|_2^2 - \frac{1}{4}\|\nabla_h\tilde{\phi}^{n-1}\|_2^2.
\end{aligned} \tag{5.15}$$

For the inner product associated with the expansive part, the following inequality is available:

$$\begin{aligned}
\theta_0\langle 3\tilde{\phi}^n - \tilde{\phi}^{n-1}, \tilde{\phi}^{n+1}\rangle_\Omega &\le \theta_0\|3\tilde{\phi}^n - \tilde{\phi}^{n-1}\|_{-1,h}\|\nabla_h\tilde{\phi}^{n+1}\|_2 \\
&\le \theta_0^2\varepsilon^{-2}\|3\tilde{\phi}^n - \tilde{\phi}^{n-1}\|_{-1,h}^2 + \frac{\varepsilon^2}{4}\|\nabla_h\tilde{\phi}^{n+1}\|_2^2 \\
&\le \theta_0^2\varepsilon^{-2}(12\|\tilde{\phi}^n\|_{-1,h}^2 + 4\|\tilde{\phi}^{n-1}\|_{-1,h}^2) + \frac{\varepsilon^2}{4}\|\nabla_h\tilde{\phi}^{n+1}\|_2^2.
\end{aligned} \tag{5.16}$$

The term associated with the truncation error can be controlled in a standard way:

$$2\langle\tau^n,\tilde{\phi}^{n+1}\rangle_{-1,h}\le 2\|\tau^n\|_{-1,h}\|\tilde{\phi}^{n+1}\|_{-1,h}\le\|\tau^n\|^2_{-1,h}+\|\tilde{\phi}^{n+1}\|^2_{-1,h}. \tag{5.17}$$

The rest work will be focused on the nonlinear error estimates. For the error term $\mathcal{N}_1^n$, we begin with the following observation: we can write $\mathcal{N}_1^n=\mathcal{N}_{11}^n+\mathcal{N}_{12}^n$, where

$$\begin{aligned}\mathcal{N}_{11}^n&=G^1_{1+\phi^n}(1+\Phi_N^{n+1})-G^1_{1+\phi^n}(1+\phi^{n+1}),\\ \mathcal{N}_{12}^n&=G^1_{1+\Phi_N^{n+1}}(1+\Phi_N^n)-G^1_{1+\Phi_N^{n+1}}(1+\phi^n),\end{aligned} \tag{5.18}$$

and $G_a^1(x)$ is as defined in (2.12). Since $G_a^1(x)$ is a monotonically increasing function of $x>0$ (Lemma 2.3), we see that

$$\langle\mathcal{N}_{11}^n,\tilde{\phi}^{n+1}\rangle_\Omega=\langle G^1_{1+\phi^n}(1+\Phi_N^{n+1})-G^1_{1+\phi^n}(1+\phi^{n+1}),\Phi_N^{n+1}-\phi^{n+1}\rangle_\Omega\ge 0. \tag{5.19}$$

For the $\mathcal{N}_{12}^n$ error term, we apply the intermediate value theorem to obtain

$$\begin{aligned}\mathcal{N}_{12}^n&=G^1_{1+\Phi_N^{n+1}}(1+\Phi_N^n)-G^1_{1+\Phi_N^{n+1}}(1+\phi^n)\\ &=(G^1_{1+\Phi_N^{n+1}})'(\eta)(\Phi_N^n-\phi^n),\end{aligned} \tag{5.20}$$

for some η that is between $1+\Phi_N^n$ and $1+\phi^n$. Meanwhile, by property (3) in Lemma 2.3, we conclude that

$$(G^1_{1+\Phi_N^{n+1}})'(\eta)=\frac{1}{2\xi_1}, \tag{5.21}$$

for some ξ_1 that is between $1+\Phi_N^{n+1}$ and η. Now, since ξ_1 is between $1+\Phi_N^{n+1}$ and η, and since η is between $1+\Phi_N^n$ and $1+\phi^n$, the following bound is available

$$\left|\frac{1}{\xi_1}\right|\le\max\left\{\frac{1}{1+\Phi_N^{n+1}},\frac{1}{1+\Phi_N^n},\frac{1}{1+\phi^n}\right\}\le\frac{4}{\epsilon_0}, \tag{5.22}$$

where the separation properties (5.4) and (5.13) have been recalled. Then we arrive at

$$|\mathcal{N}_{12}^n|=\left|(G^1_{1+\Phi_N^{n+1}})'(\eta)\right|\cdot|\tilde{\phi}^n|=\left|\frac{1}{2\xi_1}\right|\cdot|\tilde{\phi}^n|\le\frac{2}{\epsilon_0}|\tilde{\phi}^n|. \tag{5.23}$$

Based on this point-wise bound, the following inequality is available

$$\langle\mathcal{N}_{12}^n,\tilde{\phi}^{n+1}\rangle_\Omega\ge-\frac{2}{\epsilon_0}|\langle\tilde{\phi}^n,\tilde{\phi}^{n+1}\rangle_\Omega|\ge-\frac{1}{\epsilon_0}(\|\tilde{\phi}^n\|_2^2+\|\tilde{\phi}^{n+1}\|_2^2). \tag{5.24}$$

Subsequently, a combination of (5.19) and (5.24) yields

$$\langle\mathcal{N}_1^n,\tilde{\phi}^{n+1}\rangle_\Omega\ge-\frac{1}{\epsilon_0}(\|\tilde{\phi}^n\|_2^2+\|\tilde{\phi}^{n+1}\|_2^2). \tag{5.25}$$

The estimate for the $\mathcal{N}_2$ term could be similarly derived; the technical details are left to interested readers:

$$\langle \mathcal{N}_2^n, \tilde{\phi}^{n+1} \rangle_\Omega \geq -\frac{1}{\epsilon_0}(\|\tilde{\phi}^n\|_2^2 + \|\tilde{\phi}^{n+1}\|_2^2). \tag{5.26}$$

For the nonlinear inner product associated with the artificial regularization, the fact that $-1 < \phi^{n+1} < 1$, $-1 < \Phi_N^{n+1} < 1$ (at a point-wise level) yields the following results:

$$\langle \mathcal{N}_3^n, \tilde{\phi}^{n+1} \rangle_\Omega = \langle \ln(1+\Phi_N^{n+1}) - \ln(1+\phi^{n+1}), \tilde{\phi}^{n+1} \rangle_\Omega \geq 0, \tag{5.27}$$

$$\langle \mathcal{N}_5^n, \tilde{\phi}^{n+1} \rangle_\Omega = -\langle \ln(1-\Phi_N^{n+1}) - \ln(1-\phi^{n+1}), \tilde{\phi}^{n+1} \rangle_\Omega \geq 0, \tag{5.28}$$

due to the fact that the natural logarithm is a monotonically increasing function. The estimate for the $\mathcal{N}_4^n$ term is similar to that of $\mathcal{N}_{12}^n$:

$$\mathcal{N}_4^n = -\ln(1+\Phi_N^n) + \ln(1+\phi^n) = -\frac{1}{\xi_2}\tilde{\phi}^n, \tag{5.29}$$

for some ξ_2 between $1+\Phi_N^n$ and $1+\phi^n$. But

$$\left|\frac{1}{\xi_2}\right| \leq \max\left\{\frac{1}{1+\Phi_N^n}, \frac{1}{1+\phi^n}\right\} \leq \frac{4}{\epsilon_0}. \tag{5.30}$$

Thus,

$$|\mathcal{N}_4^n| = \left|\frac{1}{\xi_2}\right| \cdot |\tilde{\phi}^n| \leq \frac{4}{\epsilon_0}|\tilde{\phi}^n|. \tag{5.31}$$

We conclude that

$$\langle \mathcal{N}_4^n, \tilde{\phi}^{n+1} \rangle_\Omega \geq -\frac{4}{\epsilon_0}|\langle \tilde{\phi}^n, \tilde{\phi}^{n+1} \rangle_\Omega| \geq -\frac{2}{\epsilon_0}(\|\tilde{\phi}^n\|_2^2 + \|\tilde{\phi}^{n+1}\|_2^2). \tag{5.32}$$

The lower bound for $\langle \mathcal{N}_6^n, \tilde{\phi}^{n+1} \rangle_\Omega$ could be derived in the same fashion:

$$\langle \mathcal{N}_6^n, \tilde{\phi}^{n+1} \rangle_\Omega \geq -\frac{2}{\epsilon_0}(\|\tilde{\phi}^n\|_2^2 + \|\tilde{\phi}^{n+1}\|_2^2). \tag{5.33}$$

Using estimates (5.15)-(5.17), (5.25)-(5.28), and (5.32) and (5.33) in (5.14) yields

$$\begin{aligned}
&\frac{1}{\Delta t}(\|\tilde{\phi}^{n+1}\|_{-1,h}^2 - \|\tilde{\phi}^n\|_{-1,h}^2) + \varepsilon^2\left(\|\nabla_h\tilde{\phi}^{n+1}\|_2^2 - \frac{1}{4}\|\nabla_h\tilde{\phi}^{n-1}\|_2^2\right) \\
\leq &\theta_0^2\varepsilon^{-2}(12\|\tilde{\phi}^n\|_{-1,h}^2 + 4\|\tilde{\phi}^{n-1}\|_{-1,h}^2) + \|\tilde{\phi}^{n+1}\|_{-1,h}^2 + \frac{3}{\epsilon_0}(\|\tilde{\phi}^n\|_2^2 + \|\tilde{\phi}^{n+1}\|_2^2) + \|\tau^n\|_{-1,h}^2,
\end{aligned} \tag{5.34}$$

provided that $\Delta t \leq \frac{1}{4}$. Moreover, for the two error terms $\|\tilde{\phi}^n\|_2^2$, $\|\tilde{\phi}^{n+1}\|_2^2$, the following bounds are available:

$$\frac{3}{\epsilon_0}\|\tilde{\phi}^k\|_2^2 \leq \frac{3}{\epsilon_0}\|\tilde{\phi}^k\|_{-1,h}\|\nabla_h\tilde{\phi}^n\|_2 \leq 9\epsilon_0^{-2}\varepsilon^{-2}\|\tilde{\phi}^k\|_{-1,h}^2 + \frac{\varepsilon^2}{4}\|\nabla_h\tilde{\phi}^k\|_2^2, \quad k = n, n+1. \tag{5.35}$$

The combination of the last estimate with (5.34) leads to

$$\begin{aligned}&\frac{1}{\Delta t}(\|\tilde{\phi}^{n+1}\|_{-1,h}^2-\|\tilde{\phi}^n\|_{-1,h}^2)+\varepsilon^2\Big(\frac{1}{2}\|\nabla_h\tilde{\phi}^{n+1}\|_2^2-\frac{1}{4}\|\nabla_h\tilde{\phi}^{n-1}\|_2^2\Big)\\ \le&(\varepsilon^{-2}(12\theta_0^2+9\epsilon_0^{-2})+1)(\|\tilde{\phi}^{n+1}\|_{-1,h}^2+\|\tilde{\phi}^n\|_{-1,h}^2+\|\tilde{\phi}^{n-1}\|_{-1,h}^2)+\|\tau^n\|_{-1,h}^2.\end{aligned}\tag{5.36}$$

As a result, an application of a discrete Gronwall inequality results in the desired convergence estimate:

$$\|\tilde{\phi}^{n+1}\|_{-1,h}+\Big(\varepsilon^2\Delta t\sum_{k=0}^{n+1}\|\nabla_h\tilde{\phi}^m\|_2^2\Big)^{1/2}\le C(\Delta t^2+h^2),\tag{5.37}$$

where $C>0$ is independent of Δt, h, and n, due to the fact that $\|\tau^n\|_{-1,h}\le C(\Delta t^2+h^2)$.

Finally, we can recover the a-priori assumption (5.11) using the error estimate (5.37). Specifically, since

$$\begin{aligned}&\|\tilde{\phi}^{n+1}\|_{-1,h}\le C(\Delta t^2+h^2),\\ &\|\nabla_h\tilde{\phi}^{n+1}\|_2\le\frac{C(\Delta t^2+h^2)}{\Delta t^{\frac{1}{2}}}\le C(\Delta t^{\frac{3}{2}}+h^{\frac{3}{2}}),\end{aligned}$$

it follows that

$$\|\tilde{\phi}^{n+1}\|_2\le\|\tilde{\phi}^{n+1}\|_{-1,h}^{\frac{1}{2}}\|\nabla_h\tilde{\phi}^{n+1}\|_2^{\frac{1}{2}}\le C(\Delta t^{\frac{7}{4}}+h^{\frac{7}{4}})\le\Delta t^{\frac{13}{8}}+h^{\frac{13}{8}},\tag{5.38}$$

provided that Δt and h are sufficiently small and the linear refinement constraint, $C_5h\le\Delta t\le C_6h$ holds. Therefore, an induction analysis could be applied. This completes the proof of Theorem 5.1. □

6 Numerical solver: Preconditioned steepest descent iteration

A preconditioned steepest descent (PSD) iteration algorithm is used to implement the proposed numerical scheme (2.9), (2.10), following the practical and theoretical framework in [31]. As proved in the positivity-preserving analysis, the numerical solution of (2.9) can be recast as a minimization of the discrete convex energy functional (3.3), which becomes the discrete variation of (3.3) set equal to zero: $\mathcal{N}_h[\phi]=f^n$, where

$$\begin{aligned}\mathcal{N}_h[\phi]:=&\Delta t(\ln(1+\phi)-\ln(1-\phi))+G^1_{1+\phi^n}(1+\phi)-G^1_{1-\phi^n}(1-\phi)\\ &+f^n-\frac{3}{4}\varepsilon^2\Delta_h\phi+\frac{1}{\Delta t}\mathcal{L}^{-1}_{\breve{\mathcal{M}}^{n+1/2}}(\phi-\phi^n).\end{aligned}\tag{6.1}$$

The essential idea of the PSD solver is to use a linearized version of the nonlinear operator as a pre-conditioner. Specifically, the preconditioner, $\mathcal{L}_h:\mathring{\mathcal{C}}_{\rm per}\to\mathring{\mathcal{C}}_{\rm per}$, is defined as

$$\mathcal{L}_h[\psi]:=\frac{1}{\Delta t}(-\Delta_h)^{-1}\psi+2\psi-\frac{3}{4}\varepsilon^2\Delta_h\psi,$$

and is a positive, symmetric operator. Specifically, this "metric" is used to find an appropriate search direction for the steepest descent solver [31]. Given the current iterate $\phi_n \in \mathcal{C}_{\text{per}}$, we define the following *search direction* problem: find $d_n \in \mathcal{C}_{\text{per}}$ such that

$$\mathcal{L}_h[d_n] = r_n - \overline{r_n}, \quad r_n := f^n - \mathcal{N}_h[\phi_n],$$

where r_n is the nonlinear residual of the n^{th} iterate ϕ_n. Of course, this equation can be efficiently solved using the Fast Fourier Transform (FFT). Subsequently, the next iterate is obtained as

$$\phi_{n+1} := \phi_n + \alpha_n d_n, \tag{6.2}$$

where $\alpha_n \in \mathbb{R}$ is the unique solution to the steepest descent line minimization problem

$$\alpha_n := \underset{\alpha\in\mathbb{R}}{\text{argmin}}\, \mathcal{J}[\phi_n + \alpha d_n] = \underset{\alpha\in\mathbb{R}}{\text{argzero}}\, \langle \mathcal{N}_h[\phi_n + \alpha d_n] - f^n, d_n\rangle_\Omega. \tag{6.3}$$

Following similar techniques reported in [31], a theoretical analysis ensures a geometric convergence of the iteration sequence. Also see [11, 16, 30, 32] for the applications of the PSD solver to various gradient flow models. In fact, although $\mathcal{J}$ is only defined over grid functions with point-wise positive values for $1+\phi$ and $1-\phi$, we notice its convexity in terms of ϕ, as well as the singular nature of the logarithmic function as $1+\phi$ or $1-\phi$ approaches the limiting value of 0. These features imply that the minimization problem (6.3) has a unique solution for α based on a similar argument as in the proof of Theorem 3.1.

7 Numerical results

7.1 Convergence tests for the numerical scheme

In this subsection we perform a numerical accuracy check for the proposed numerical scheme (2.9)-(2.10). The computational domain is chosen as $\Omega = (0,1)^2$, and the exact profile for the phase variable is set to be

$$\Phi(x,y,t) = \frac{1}{\pi}\sin(2\pi x)\cos(2\pi y)\cos(t). \tag{7.1}$$

In particular, we see that the $1+\Phi$ and $1-\Phi$ stay positive at a point-wise level, so that the computation will not cause any singularity issue. To make Φ satisfy the original PDE (1.2)-(1.3), we have to add an artificial, time-dependent forcing term. Then the proposed scheme (2.9)-(2.10) can be implemented to solve for (1.2). In addition, we have tested both the constant mobility flow, (a) $\mathcal{M}(\phi)\equiv 1$, and (b) the flow with the mobility function given by

$$\mathcal{M}(\phi) = \Big(\frac{1}{2} + \frac{1}{2}(1+\phi)(1-\phi)\Big)^{-1}. \tag{7.2}$$

Notice that this mobility function has a uniform lower bound $\mathcal{M}(\phi) \geq 1$, for $-1 < \phi < 1$. In the practical computations, a more singular lower bound could also be taken, such as

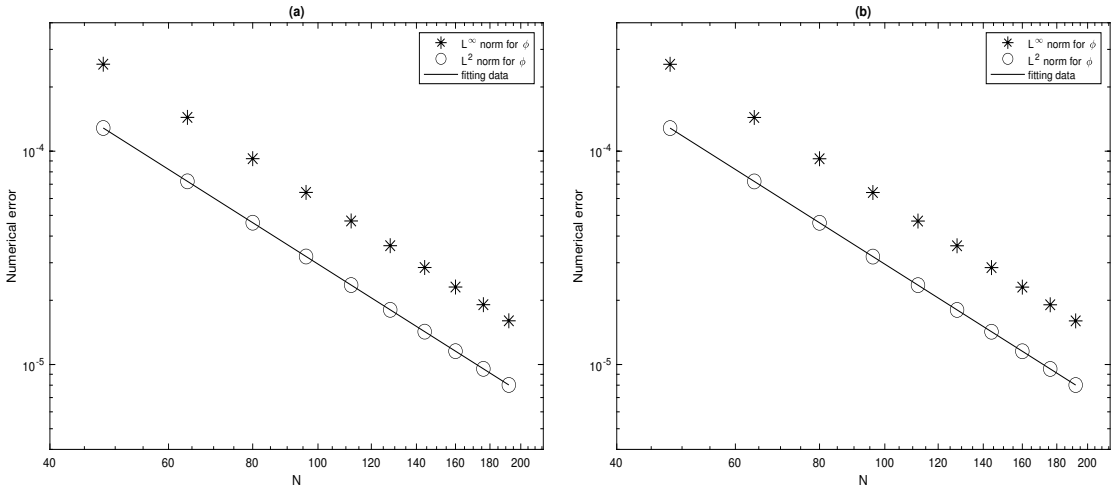

Figure 1: The discrete L_h^2 and L_h^∞ numerical errors vs. spatial resolution N for $N=48:16:192$, and the time step size is set as $\Delta t=\frac{1}{2}h$. The numerical results are obtained by the computation using the numerical scheme (2.9)-(2.10), and the surface diffusion parameter is taken to be $\varepsilon=0.5$. (a) The results with a constant mobility $\mathcal{M}(\phi)\equiv 1$. (b) The results with the mobility function given by (7.2). In both cases, the data lie roughly on curves CN^{-2}, for appropriate choices of C, confirming the full second-order accuracy of the scheme, in both time and space.

$\mathcal{M}(\phi)=\gamma(1+\phi)(1-\phi)$, while more PSD iteration steps are needed to ensure a perfect iteration convergence at each time step.

In the accuracy test for the numerical scheme, we set the time size as $\Delta t=\frac{1}{2}h$, with $h=\frac{1}{N}$, so that the second order accuracy in both time and space could be confirmed. The final time set as by $T=1$, the surface diffusion parameter is given by $\varepsilon=0.5$, while the expansive parameter is set as $\theta_0=2$. A sequence of spatial resolutions are taken as $N=48:16:192$. The expected temporal numerical accuracy assumption $e=C(\Delta t^2+h^2)$ indicates that $\ln|e|=\ln C-2\ln N$, so that we plot $\ln|e|$ vs. $\ln N$ to demonstrate the temporal convergence order. The numerical errors for both the constant mobility flow and variable mobility case (7.2) are displayed in the two plots in Fig. 1. In both cases, the fitted line shows an approximate slope of -1.9980, which verifies the second order accuracy, in both time and space.

7.2 Numerical simulation of coarsening processes

The logarithmic nonlinear term associated with the Flory-Huggins potential gives preference to many small structures. In this subsection, we perform a two-dimensional numerical simulation showing the coarsening process. The computational domain is set as $\Omega=(0,1)^2$, the expansive parameter is given by $\theta_0=3$, and the interface width parameter is taken as $\varepsilon=0.005$. The initial data are given by

$$\phi_{i,j}^0=0.1+0.05\cdot(2r_{i,j}-1),\quad r_{i,j}\text{ are uniformly distributed random numbers in }[0,1]. \tag{7.3}$$

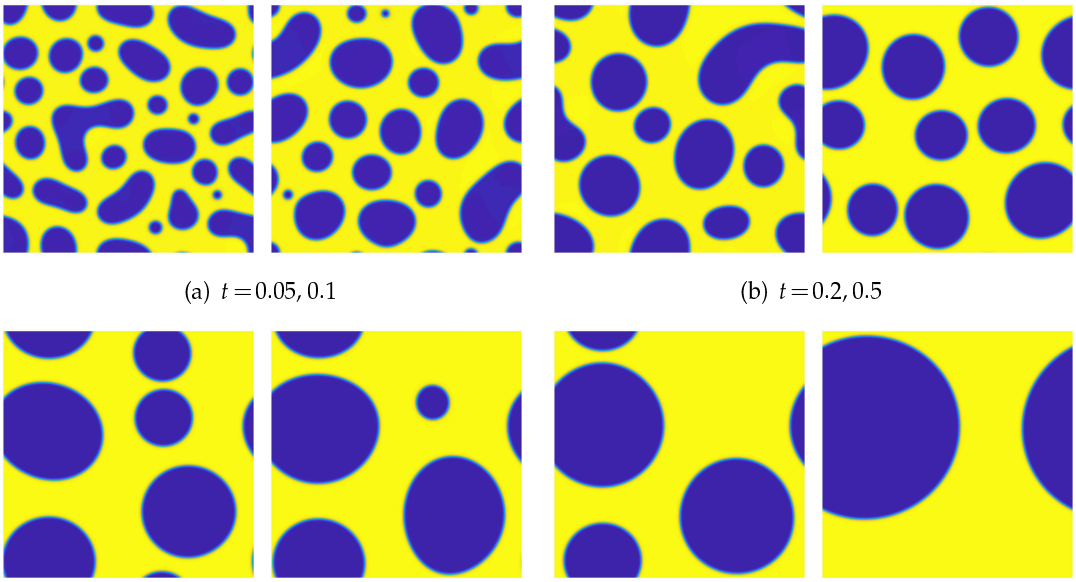

(a) $t=0.05, 0.1$ (b) $t=0.2, 0.5$

(c) $t=1, 2$ (d) $t=3, 15$

Figure 2: (Color online.) Snapshots of the phase variable ϕ at the indicated time instants over the domain $\Omega=(0,1)^2$, $\varepsilon=0.005$, $\theta_0=3$, with a constant mobility $\mathcal{M}\equiv 1$. Finally, there is a single structure at $t=15$.

The proposed numerical scheme (2.9)-(2.10) is implemented for this simulation. For the temporal step size Δt, we use increasing values of Δt in the time evolution: $\Delta t=5\times 10^{-5}$ on the time interval $[0,1]$, $\Delta t=10^{-4}$ on the time interval $[1,3]$, $\Delta t=2\times 10^{-4}$ on the time interval $[3,7]$ and $\Delta t=5\times 10^{-4}$ on the time interval $[7,15]$. Whenever a new time step size is applied, we initiate the two-step numerical scheme by taking $\phi^{-1}=\phi^0$, with the initial data ϕ^0 given by the final time output of the last time period. The time snapshots of the evolution by using $\varepsilon=0.005$ are presented in Fig. 2, with significant coarsening observed in the system. At early times many small structures are present. At the final time, $t=15$, a single structure emerges, and further coarsening is not possible.

To illustrate the phase separation property for the two-dimensional Cahn-Hilliard flow, we display the maximum and minimum values of the phase variable at such a time sequence in Table 1. Although these maximum and minimum values are close to the singular limit values of 1 and -1, a safe distance, with an order of $\mathcal{O}(10^{-1})$, is clearly observed in the numerical simulation. This numerical result also agrees with the phase separation estimate established in the existing theoretical analysis [2, 20, 28, 53].

Moreover, the long time characteristics of the solution, especially the energy decay rate, are of interest to material scientists. For the epitaxial thin film growth and polynomial-approximation Cahn-Hilliard gradient models, certain theoretical analysis [44] has provided an upper bound of the energy decay rate as $t^{-1/3}$, and some numerical experiments have also demonstrated such a scaling law [15, 17]. However, for the Cahn-Hilliard flow

Table 1: The maximum and minimum values of the phase variable ϕ at the indicated time instants over the domain $\Omega=(0,1)^2$, $\varepsilon=0.005$, $\theta_0=3$, with a constant mobility $\mathcal{M}\equiv 1$.

Time instants	the maximum value	the minimum value
$t_1=0.05$	0.8644627	-0.8799553
$t_2=0.1$	0.8607157	-0.8805562
$t_3=0.2$	0.8616231	-0.8661328
$t_4=0.5$	0.8554958	-0.8637321
$t_5=1$	0.856433	-0.8630059
$t_6=2$	0.8566435	-0.8661082
$t_7=3$	0.8564997	-0.8619818
$t_8=15$	0.8572049	-0.8599514

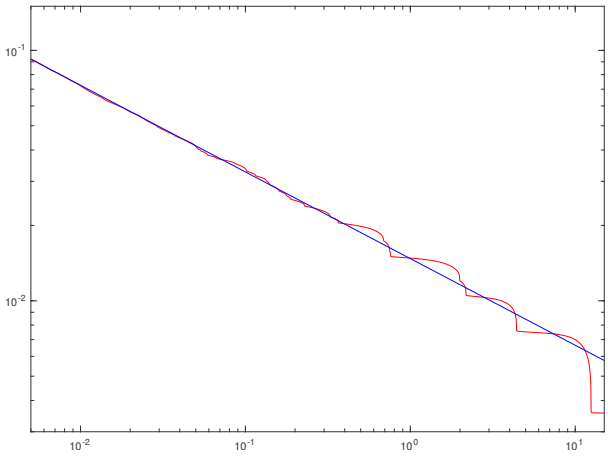

Figure 3: Log-log plot of the temporal evolution the energy E_h for $\varepsilon=0.005$, $\theta_0=3$, with a constant mobility $\mathcal{M}\equiv 1$. The energy decreases like $a_e t^{b_e}$ until saturation. The red lines represent the energy plot obtained by the simulations, while the straight lines are obtained by least squares approximations to the energy data. The least squares fit is only taken for the linear part of the calculated data, only up to about time $t=100$. The fitted line has the form $a_e t^{b_e}$, with $a_e=0.01474$, $b_e=-0.3460$.

with Flory-Huggins logarithmic energy potential, such a theoretical justification has not been available yet. In this article, we provide some numerical evidences on this issue. Fig. 3 presents the log-log plot for the energy versus time, with the given physical parameters, in which the discrete E_h is defined as (4.1). The detailed scaling "exponent" is obtained using least squares fits of the computed data up to time $t=100$. A clear observation of the $a_e t^{b_e}$ scaling law can be made, with $a_e=0.01474$, $b_e=-0.3460$. It is amazing to obtain an energy dissipation scaling index for the Flory-Huggins Cahn-Hilliard flow in the long time numerical simulation, which is close to the $t^{-1/3}$ scaling observed in the polynomial approximation model.

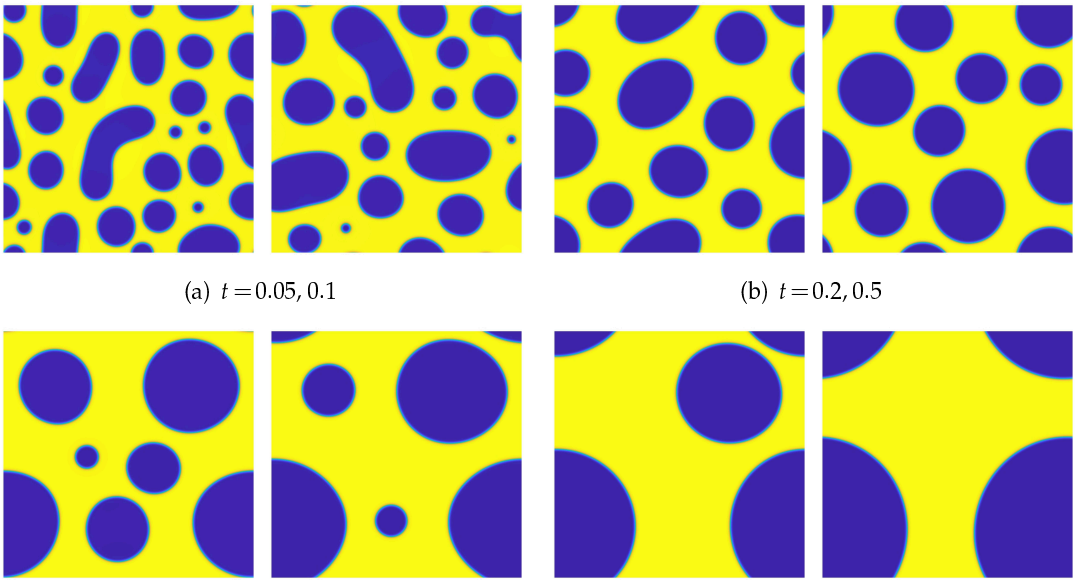

(a) $t=0.05, 0.1$ (b) $t=0.2, 0.5$

(c) $t=1, 2$ (d) $t=3, 7$

Figure 4: (Color online.) Snapshots of the phase variable ϕ at the indicated time instants over the domain $\Omega=(0,1)^2$, $\varepsilon=0.005$, $\theta_0=3$, with the solution-dependent mobility (7.2). Finally, there is a single structure at $t=7$.

To demonstrate the robustness of the proposed numerical scheme (2.9)-(2.10) , we have also performed a numerical simulation with a solution-dependent mobility function (7.2), using the same random initial data (7.3) and the physical parameters: $\Omega=(0,1)^2$, $\varepsilon=0.005$, and $\theta_0=3$. For the solution-dependent mobility simulation, we use similar increasing values of the temporal time step Δt: $\Delta t=5\times 10^{-5}$ on the time interval $[0,1]$, $\Delta t=10^{-4}$ on the time interval $[1,7]$. The time snapshots of the evolution by using are presented in Fig. 4, with significant coarsening observed in the system. At early times many small structures are present. More importantly, with the solution-dependent mobility function, it seems that the coarsening process is faster than the constant mobility case. At the final time, $t=7$, a single structure emerges, in comparison with the final time $t=15$ in the constant mobility case.

Similarly, the maximum and minimum values of the phase variable at such a time sequence is displayed in Table 2. Again, a safe distance, with an order of $\mathcal{O}(10^{-1})$, is clearly observed between the numerical solution and the singular limit values, and this numerical result agrees with the existing theoretical analysis of the phase separation estimate for the two-dimensional Cahn-Hilliard flow.

Fig. 5 presents the log-log plot for the energy versus time, with the given physical parameters, using the solution-dependent mobility function (7.2). The coarsening process is similar to the constant-mobility case, while the time scale to reach the steady state is little shorter. A scaling law of $a_e t^{b_e}$ scaling law is also available, with $a_e=0.01406$,

Table 2: The maximum and minimum values of the phase variable ϕ at the indicated time instants over the domain $\Omega=(0,1)^2$, $\varepsilon=0.005$, $\theta_0=3$, with the solution-dependent mobility (7.2).

Time instants	the maximum value	the minimum value
$t_1=0.05$	0.8619546	-0.8801955
$t_2=0.1$	0.8627765	-0.87967
$t_3=0.2$	0.8564543	-0.8648476
$t_4=0.5$	0.8552953	-0.8646686
$t_5=1$	0.8564688	-0.8692348
$t_6=2$	0.8567849	-0.8664668
$t_7=3$	0.8569047	-0.8611875
$t_8=7$	0.8572687	-0.8600034

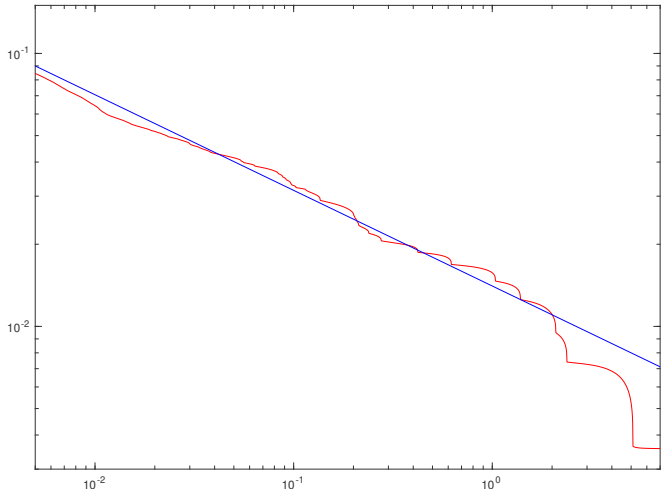

Figure 5: Log-log plot of the temporal evolution the energy E_h for $\varepsilon=0.005$, $\theta_0=3$, with the solution-dependent mobility (7.2). The energy decreases like $a_e t^{b_e}$ until saturation. The red lines represent the energy plot obtained by the simulations, while the straight lines are obtained by least squares approximations to the energy data. The least squares fit is only taken for the linear part of the calculated data, only up to about time $t=100$. The fitted line has the form $a_e t^{b_e}$, with $a_e=0.01406$, $b_e=-0.3503$.

$b_e=-0.3502$. Such a scaling law is very close to the constant-mobility case, at least for the coarsening process up to $t=100$.

Moreover, to explore the dependence of phase separation property of the numerical solution on the expansive parameter θ_0, we perform a numerical simulation with a larger value, $\theta_0=3.5$, using the proposed numerical scheme (2.9)-(2.10). For simplicity, we take a constant mobility $\mathcal{M}(\phi)\equiv 1$, while a solution-dependent mobility flow could be similarly computed. Due to the larger value of θ_0, the gradient flow becomes more challenging to compute, and we have to take smaller values of temporal step size Δt to make the

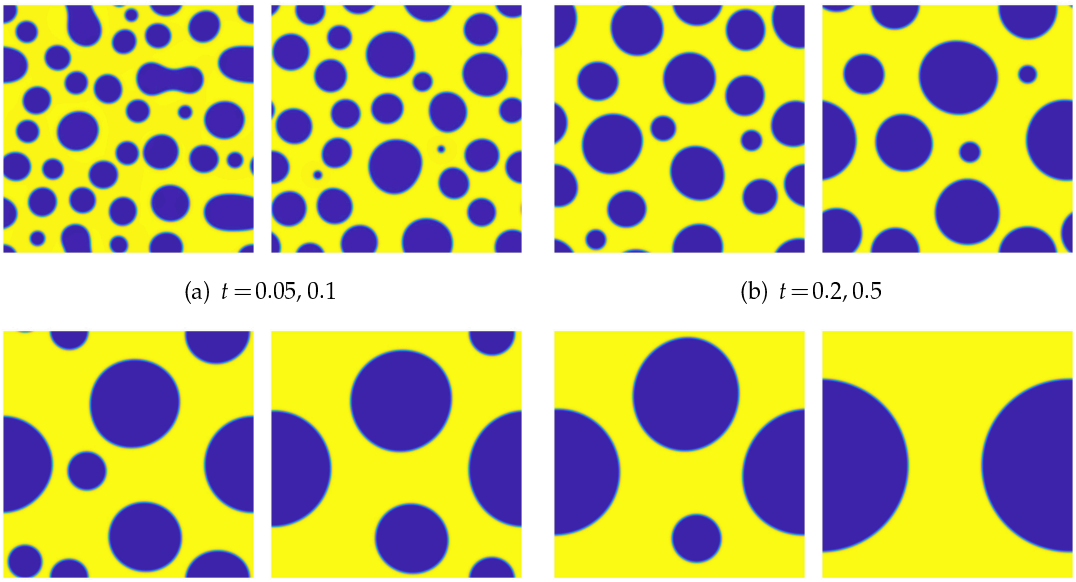

(a) $t=0.05, 0.1$ (b) $t=0.2, 0.5$

(c) $t=1, 2$ (d) $t=3, 15$

Figure 6: (Color online.) Snapshots of the phase variable ϕ at the indicated time instants over the domain $\Omega=(0,1)^2$, $\varepsilon=0.005$, $\theta_0=3.5$, with a constant mobility $\mathcal{M}\equiv 1$. Finally, there is a single structure at $t=15$.

numerical solution stable: $\Delta t=2\times 10^{-5}$ on the time interval $[0,0.5]$, $\Delta t=5\times 10^{-5}$ on the time interval $[0.5,1]$, $\Delta t=10^{-4}$ on the time interval $[1,3]$, $\Delta t=2\times 10^{-4}$ on the time interval $[3,7]$ and $\Delta t=5\times 10^{-4}$ on the time interval $[7,15]$. The time snapshots of the evolution by using $\varepsilon=0.005$ are presented in Fig. 6, with more complicated structures observed in the system. Similarly, at the final time, $t=15$, a single structure emerges, and further coarsening is not possible.

The maximum and minimum values of the phase variable, with a larger expansive parameter $\theta_0=3.5$, is displayed in Table 3. Due to the larger value of the expansive parameter, we see that the maximum and minimum values are much close to the singular limit values of 1 and -1; more precisely, the numerical solutions stays in the range of approximately $[-0.95,0.95]$. On the other hand, the numerical stability and positivity-preserving property has been well preserved in the numerical solution, although the gradient flow becomes more singular. This numerical simulation provides another evidence of the robustness of the proposed second order scheme.

Fig. 7 presents the log-log plot for the energy versus time, with $\varepsilon=0.005$, $\theta_0=3.5$ and $\mathcal{M}(\phi)\equiv 1$. A scaling law of $a_e t^{b_e}$ scaling law is also available, with $a_e=0.03306$, $b_e=-0.2738$.

With increasing values of expansive parameter θ_0, we have to take smaller temporal step size is needed in the numerical solution, and a closer distance to the singular limit values of 1 and -1 is expected. Meanwhile, the existing numerical evidence has

Table 3: The maximum and minimum values of the phase variable ϕ at the indicated time instants over the domain $\Omega=(0,1)^2$, $\varepsilon=0.005$, $\theta_0=3.5$, with a constant mobility $\mathcal{M}\equiv 1$.

Time instants	the maximum value	the minimum value
$t_1=0.05$	0.9259174	-0.9355966
$t_2=0.1$	0.9213976	-0.9409601
$t_3=0.2$	0.9216448	-0.9318636
$t_4=0.5$	0.9222424	-0.9326683
$t_5=1$	0.9225917	-0.9288619
$t_6=2$	0.9229	-0.9277333
$t_7=3$	0.9230522	-0.9274924
$t_8=15$	0.9233391	-0.9251632

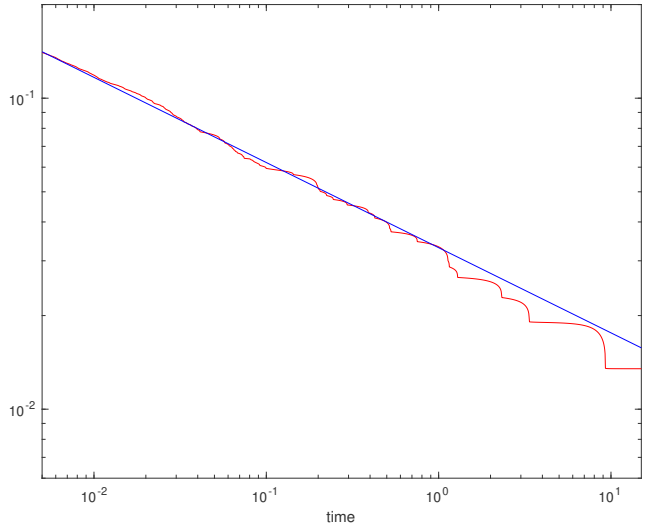

Figure 7: Log-log plot of the temporal evolution the energy E_h for $\varepsilon=0.005$, $\theta_0=3.5$, and $\mathcal{M}\equiv 1$. The energy decreases like $a_e t^{b_e}$ until saturation. The red lines represent the energy plot obtained by the simulations, while the straight lines are obtained by least squares approximations to the energy data. The least squares fit is only taken for the linear part of the calculated data, only up to about time $t=100$. The fitted line has the form $a_e t^{b_e}$, with $a_e=0.03306$, $b_e=-0.2738$.

demonstrated the efficiency of the proposed numerical scheme to preserve the positivity property.

8 Concluding remarks

In this paper we have presented and analyzed a second order accurate, positivity preserving, energy stable finite difference scheme for the Cahn-Hilliard model with a log-

arithmic Flory Huggins energy potential. A modified Crank-Nicolson approximation, in the form of $\frac{F(1\pm\phi^{n+1})-F(1\pm\phi^n)}{\phi^{n+1}-\phi^n}$ is applied to the logarithmic nonlinear term, while the expansive term is updated by a second order Adams-Bashforth explicit extrapolation formula, and an alternate temporal stencil, with coefficient distribution of $\frac{3}{4}$ and $\frac{1}{4}$ at t_{n+1} and t_{n-1}, is used for the surface diffusion term. A nonlinear artificial regularization term, in the form of $\Delta t(\ln(1\pm\phi^{n+1})-\ln(1\pm\phi^n))$, is added in the numerical scheme. Such a regularization term ensures the positivity-preserving property for the logarithmic arguments, i.e., the phase variable is always between -1 and 1, at a point-wise level. In particular, the singular nature of the logarithmic term around the values of -1 and $+1$ prevents the numerical solution reaching these singular values. A modified energy stability has been theoretically justified, as a result of careful estimate. In comparison with the BDF2 approach, the proposed Crank-Nicolson-type discretization has an advantage to deal with the non-constant mobility case while preserving an energy stability. In addition, an optimal rate convergence in the $L^\infty_{\Delta t}(0,T;H_h^{-1})\cap L^2_{\Delta t}(0,T;H_h^1)$ norm has been established, with the help of a linearized stability analysis. Some numerical results are presented, which demonstrate the robustness and efficiency of the numerical solver. A successful numerical simulation of the solution-dependent mobility flow makes a more significant contribution.

Acknowledgments

This work is supported in part by the grants NSFC 12071090 (W. Chen), NSF DMS-2012669 (C. Wang), NSFC 11871159, Guangdong Provincial Key Laboratory for Computational Science and Material Design 2019B030301001 (X. Wang), and NSF DMS-1719854, DMS-2012634 (S. Wise). C. Wang also thanks the Key Laboratory of Mathematics for Nonlinear Sciences, Fudan University, for the support.

References

[1] H. Abels. On a diffuse interface model for two-phase flows of viscous, incompressible fluids with matched densities. *Arch. Ration. Mech. Anal.*, 194(2):463–506, 2009.

[2] H. Abels and M. Wilke. Convergence to equilibrium for the Cahn-Hilliard equation with a logarithmic free energy. *Nonlinear Anal.*, 67:3176–3193, 2007.

[3] S. M. Allen and J. W. Cahn. A microscopic theory for antiphase boundary motion and its application to antiphase domain coarsening. *Acta. Metall.*, 27:1085, 1979.

[4] J. Barrett and J. Blowey. Finite element approximation of the Cahn-Hilliard equation with concentration dependent mobility. *Math. Comp.*, 68:487–517, 1999.

[5] A. Baskaran, Z. Hu, J. Lowengrub, C. Wang, S.M. Wise, and P. Zhou. Energy stable and efficient finite-difference nonlinear multigrid schemes for the modified phase field crystal equation. *J. Comput. Phys.*, 250:270–292, 2013.

[6] A. Baskaran, J. Lowengrub, C. Wang, and S. Wise. Convergence analysis of a second order convex splitting scheme for the modified phase field crystal equation. *SIAM J. Numer. Anal.*, 51:2851–2873, 2013.

[7] J.F. Blowey, M.I.M. Copetti, and C.M. Elliott. Numerical analysis of a model for phase separation of a multi-component alloy. *IMA J. Numer. Anal.*, 16:111–139, 1996.
[8] J.W. Cahn, C.M. Elliott, and A. Novick-Cohen. The Cahn-Hilliard equation with a concentration dependent mobility: Motion by minus the Laplacian of the mean curvature. *Europ. J. Appl. Math.*, 7:287–301, 1996.
[9] J.W. Cahn and J.E. Hilliard. Free energy of a nonuniform system. I. Interfacial free energy. *J. Chem. Phys.*, 28:258–267, 1958.
[10] W. Chen, W. Feng, Y. Liu, C. Wang, and S.M. Wise. A second order energy stable scheme for the Cahn-Hilliard-Hele-Shaw equation. *Discrete Contin. Dyn. Syst. Ser. B*, 24(1):149–182, 2019.
[11] W. Chen, C. Wang, S. Wang, X. Wang, and S. Wise. Energy stable numerical schemes for a ternary Cahn-Hilliard system. *J. Sci. Comput.*, 84:27, 2020.
[12] W. Chen, C. Wang, X. Wang, and S.M. Wise. A linear iteration algorithm for energy stable second order scheme for a thin film model without slope selection. *J. Sci. Comput.*, 59:574–601, 2014.
[13] W. Chen, C. Wang, X. Wang, and S.M. Wise. Positivity-preserving, energy stable numerical schemes for the Cahn-Hilliard equation with logarithmic potential. *J. Comput. Phys.: X*, 3:100031, 2019.
[14] W. Chen, X. Wang, Y. Yan, and Z. Zhang. A second order BDF numerical scheme with variable steps for the Cahn-Hilliard equation. *SIAM J. Numer. Anal.*, 57:495–525, 2019.
[15] K. Cheng, W. Feng, C. Wang, and S.M. Wise. An energy stable fourth order finite difference scheme for the Cahn-Hilliard equation. *J. Comput. Appl. Math.*, 362:574–595, 2019.
[16] K. Cheng, C. Wang, and S.M. Wise. An energy stable Fourier pseudo-spectral numerical scheme for the square phase field crystal equation. *Commun. Comput. Phys.*, 26:1335–1364, 2019.
[17] K. Cheng, C. Wang, S.M. Wise, and X. Yue. A second-order, weakly energy-stable pseudo-spectral scheme for the Cahn-Hilliard equation and its solution by the homogeneous linear iteration method. *J. Sci. Comput.*, 69:1083–1114, 2016.
[18] L. Cherfils, A. Miranville, and S. Zelik. The Cahn-Hilliard equation with logarithmic potentials. *Milan J. Math.*, 79:561–596, 2011.
[19] M.I.M. Copetti and C.M. Elliott. Numerical analysis of the Cahn-Hilliard equation with a logarithmic free energy. *Numer. Math.*, 63:39–65, 1992.
[20] A. Debussche and L. Dettori. On the Cahn-Hilliard equation with a logarithmic free energy. *Nonlinear Anal.*, 24:1491–1514, 1995.
[21] A. Diegel, C. Wang, X. Wang, and S.M. Wise. Convergence analysis and error estimates for a second order accurate finite element method for the Cahn-Hilliard-Navier-Stokes system. *Numer. Math.*, 137:495–534, 2017.
[22] A. Diegel, C. Wang, and S.M. Wise. Stability and convergence of a second order mixed finite element method for the Cahn-Hilliard equation. *IMA J. Numer. Anal.*, 36:1867–1897, 2016.
[23] M. Doi. *Soft Matter Physics*. Oxford University Press, Oxford, UK, 2013.
[24] L. Dong, W. Feng, C. Wang, S.M. Wise, and Z. Zhang. Convergence analysis and numerical implementation of a second order numerical scheme for the three-dimensional phase field crystal equation. *Comput. Math. Appl.*, 75(6):1912–1928, 2018.
[25] L. Dong, C. Wang, S. Wise, and Z. Zhang. A positivity-preserving, energy stable scheme for a ternary Cahn-Hilliard system with the singular interfacial parameters. *J. Comput. Phys.*, 442:110451, 2021.
[26] L. Dong, C. Wang, H. Zhang, and Z. Zhang. A positivity-preserving, energy stable and con-

vergent numerical scheme for the Cahn-Hilliard equation with a Flory-Huggins-deGennes energy. *Commun. Math. Sci.*, 17:921–939, 2019.

[27] L. Dong, C. Wang, H. Zhang, and Z. Zhang. A positivity-preserving second-order BDF scheme for the Cahn-Hilliard equation with variable interfacial parameters. *Commun. Comput. Phys.*, 28:967–998, 2020.

[28] C.M. Elliott and H. Garcke. On the Cahn-Hilliard equation with degenerate mobility. *SIAM J. Math. Anal.*, 27:404, 1996.

[29] X. Fan, J. Kou, Z. Qiao, and S. Sun. A componentwise convex splitting scheme for diffuse interface models with van der Waals and Peng-Robinson equations of state. *SIAM J. Sci. Comput.*, 39:B1–B28, 2017.

[30] W. Feng, Z. Guan, J.S. Lowengrub, C. Wang, S.M. Wise, and Y. Chen. A uniquely solvable, energy stable numerical scheme for the functionalized Cahn-Hilliard equation and its convergence analysis. *J. Sci. Comput.*, 76(3):1938–1967, 2018.

[31] W. Feng, A.J. Salgado, C. Wang, and S.M. Wise. Preconditioned steepest descent methods for some nonlinear elliptic equations involving p-Laplacian terms. *J. Comput. Phys.*, 334:45–67, 2017.

[32] W. Feng, C. Wang, S.M. Wise, and Z. Zhang. A second-order energy stable Backward Differentiation Formula method for the epitaxial thin film equation with slope selection. *Numer. Methods Partial Differential Equations*, 34:1975–2007, 2018.

[33] A. Giorgini, M. Grasselli, and A. Miranville. The Cahn-Hiliard-Ono equation with singular potential. *Math. Models Methods Appl. Sci.*, 27:2485–2510, 2017.

[34] A. Giorgini, M. Grasselli, and H. Wu. The Cahn-Hilliard-Hele-Shaw system with singular potential. *Ann. Inst. H. Poincare Anal. Non Lineaire*, 35:1079–1118, 2018.

[35] Z. Guan, J.S. Lowengrub, and C. Wang. Convergence analysis for second order accurate schemes for the periodic nonlocal Allen-Cahn and Cahn-Hilliard equations. *Math. Methods Appl. Sci.*, 40(18):6836–6863, 2017.

[36] Z. Guan, J.S. Lowengrub, C. Wang, and S.M. Wise. Second-order convex splitting schemes for nonlocal Cahn-Hilliard and Allen-Cahn equations. *J. Comput. Phys.*, 277:48–71, 2014.

[37] J. Guo, C. Wang, S.M. Wise, and X. Yue. An H^2 convergence of a second-order convex-splitting, finite difference scheme for the three-dimensional Cahn-Hilliard equation. *Commu. Math. Sci.*, 14:489–515, 2016.

[38] D. Han and X. Wang. A second order in time, uniquely solvable, unconditionally stable numerical scheme for Cahn-Hilliard-Navier-Stokes equation. *J. Comput. Phys.*, 290:139–156, 2015.

[39] Y. Hao, Q. Huang, and C. Wang. A third order BDF energy stable linear scheme for the no-slope-selection thin film model. *Commun. Comput. Phys.*, 29:905–929, 2021.

[40] Z. Hu, S.M. Wise, C. Wang, and J. Lowengrub. Stable and efficient finite-difference nonlinear-multigrid schemes for the phase-field crystal equation. *J. Comput. Phys.*, 228:5323–5339, 2009.

[41] D. Jeong and J. Kim. A practical numerical scheme for the ternary Cahn-Hilliard system with a logarithmic free energy. *Physica A*, 442:510–522, 2016.

[42] D. Jeong, S. Lee, and J. Kim. An efficient numerical method for evolving microstructures with strong elastic inhomogeneity. *Model. Simulation Material Sci. Eng.*, 23:045007, 2015.

[43] H. Jia, Y. Guo, M. Li, Y. Huang, and G. Feng. Decoupled, energy stable numerical scheme for the Cahn-Hilliard-Hele-Shaw system with logarithmic Flory-Huggins potential. *Commun. Comput. Phys.*, 27(4):1053–1075, 2020.

[44] R.V. Kohn and X. Yan. Upper bound on the coarsening rate for an epitaxial growth model.

Comm. Pure Appl. Math., 56:1549–1564, 2003.
[45] D. Li and T. Tang. Stability of the semi-implicit method for the Cahn-Hilliard equation with logarithmic potentials. *Ann. Appl. Math.*, 37:31–60, 2021.
[46] W. Li, W. Chen, C. Wang, Y. Yan, and R. He. A second order energy stable linear scheme for a thin film model without slope selection. *J. Sci. Comput.*, 76:1905–1937, 2018.
[47] X. Li, Z. Qiao, and H. Zhang. An unconditionally energy stable finite difference scheme for a stochastic Cahn-Hilliard equation. *Sci. China Math.*, 59:1815–1834, 2016.
[48] H. Liao, T. Tang, and T. Zhou. On energy stable, maximum-principle preserving, second-order BDF scheme with variable steps for the Allen-Cahn equation. *SIAM J. Numer. Anal.*, 58:2294–2314, 2020.
[49] C. Liu, C. Wang, and Y. Wang. A structure-preserving, operator splitting scheme for reaction-diffusion equations with detailed balance. *J. Comput. Phys.*, 436:110253, 2021.
[50] C. Liu, C. Wang, S.M. Wise, X. Yue, and S. Zhou. A positivity-preserving, energy stable and convergent numerical scheme for the Poisson-Nernst-Planck system. *Math. Comp.*, 90:2071–2106, 2021.
[51] X. Meng, Z. Qiao, C. Wang, and Z. Zhang. Artificial regularization parameter analysis for the no-slope-selection epitaxial thin film model. *CSIAM Trans. Appl. Math.*, 1:441–462, 2020.
[52] A. Miranville. On a phase-field model with a logarithmic nonlinearity. *Appl. Math.*, 57:215–229, 2012.
[53] A. Miranville and S. Zelik. Robust exponential attractors for Cahn-Hilliard type equations with singular potentials. *Math. Methods Appl. Sci.*, 27:545–582, 2004.
[54] Q. Peng. A convex-splitting scheme for a diffuse interface model with Peng-Robinson equation of state. *Adv. Appl. Math. Mech.*, 9(5):1162–1188, 2018.
[55] Q. Peng, H. Li, and Z. Xu. Energy stable linear schemes for mass-conserved gradient flows with Peng-Robinson equation of state. *East Asian J. Appl. Math.*, 9:212–232, 2019.
[56] Q. Peng, Z. Qiao, and S. Sun. Stability and convergence analysis of second-order schemes for a diffuse interface model with Peng-Robinson equation of state. *J. Comput. Math.*, 35(6):737–765, 2017.
[57] Y. Qian, C. Wang, and S. Zhou. A positive and energy stable numerical scheme for the Poisson-Nernst-Planck-Cahn-Hilliard equations with steric interactions. *J. Comput. Phys.*, 426:109908, 2021.
[58] Z. Qiao and S. Sun. Two-phase fluid simulation using a diffuse interface model with Peng-Robinson equation of state. *SIAM J. Sci. Comput.*, 36:B708–B728, 2014.
[59] J. Shen, C. Wang, X. Wang, and S.M. Wise. Second-order convex splitting schemes for gradient flows with Ehrlich-Schwoebel type energy: Application to thin film epitaxy. *SIAM J. Numer. Anal.*, 50:105–125, 2012.
[60] C. Wang and S.M. Wise. An energy stable and convergent finite-difference scheme for the modified phase field crystal equation. *SIAM J. Numer. Anal.*, 49:945–969, 2011.
[61] C. Wight and J. Zhao. Solving Allen-Cahn and Cahn-Hilliard equations using the adaptive physics informed neural networks. *Commun. Comput. Phys.*, 29(3):930–954, 2021.
[62] S.M. Wise. Unconditionally stable finite difference, nonlinear multigrid simulation of the Cahn-Hilliard-Hele-Shaw system of equations. *J. Sci. Comput.*, 44:38–68, 2010.
[63] S.M. Wise, C. Wang, and J.S. Lowengrub. An energy stable and convergent finite-difference scheme for the phase field crystal equation. *SIAM J. Numer. Anal.*, 47:2269–2288, 2009.
[64] Y. Yan, W. Chen, C. Wang, and S.M. Wise. A second-order energy stable BDF numerical scheme for the Cahn-Hilliard equation. *Commun. Comput. Phys.*, 23:572–602, 2018.
[65] X. Yang and J. Zhao. On linear and unconditionally energy stable algorithms for variable

mobility Cahn-Hilliard type equation with logarithmic Flory-Huggins potential. *Commun. Comput. Phys.*, 25:703–728, 2019.

[66] M. Yuan, W. Chen, C. Wang, S. Wise, and Z. Zhang. An energy stable finite element scheme for the three-component Cahn-Hilliard-type model for macromolecular microsphere composite hydrogels. *J. Sci. Comput.*, 87:78, 2021.

[67] A. Zeitzeff, S. Esedoglu, and K. Garikipati. Variational extrapolation of implicit schemes for general gradient flows. *SIAM J. Numer. Anal.*, 58:2799–2817, 2020.

[68] J. Zhang, C. Wang, S.M. Wise, and Z. Zhang. Structure-preserving, energy stable numerical schemes for a liquid thin film coarsening model. *SIAM J. Sci. Comput.*, 43(2):A1248–A2172, 2021.